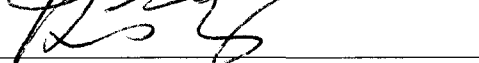RESEARCH ON DERIVING CONSISTENT LAND SURFACE TEMPERATURE
FROM THE GEOSTATIONARY OPERATIONAL ENVIRONMENTAL SATELLITE
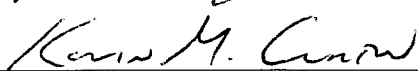SERIES

by

Li Fang
A Thesis
Submitted to the
Graduate Faculty
of
George Mason University
in Partial Fulfillment of
The Requirements for the Degree
of
Master of Science
Geographic and Cartographic Science

Committee:

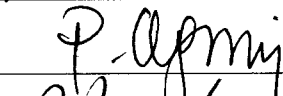_____ Dr. Donglian Sun, Thesis Director

_____ Dr. Ruixin Yang, Committee Member

_____ Dr. Kevin M. Curtin, Committee Member

_____ Dr. Peggy Agouris, Department Chair

_____ Dr. Richard Diecchio, Associate
Dean for Academic and Student
Affairs, College of Science

_____ Dr. Vikas Chandhoke, Dean,
College of Science

Date: _12/08 / 2010_____   Fall Semester 2010
George Mason University
Fairfax, VA
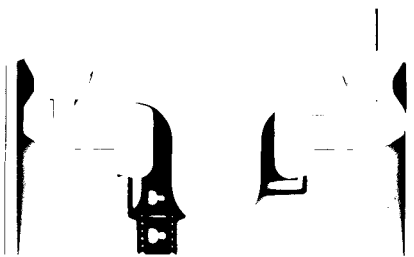
Research on Deriving Consistent Land Surface Temperature from the Geostationary
Operational Environmental Satellite Series

A thesis submitted in partial fulfillment of the requirements for the degree of Master of
Science at George Mason University

By

Li Fang
Bachelor of Science
Wuhan University, China, 2005

Director: Donglian Sun, Assistant Professor
Department of Geography and Geoinformation Science

Fall Semester 2010
George Mason University
Fairfax, VA

TABLE OF CONTENTS

List of Tables

List of Figures

Abstract

RESEARCH ON DERIVING CONSISTENT LAND SURFACE TEMPERATURE
FROM THE GEOSTATIONARY OPERATIONAL ENVIRONMENTAL SATELLITE
SERIES

Li FANG, MS

George Mason University, 2011

Thesis Director: Dr. Donglian SUN

Geostationary Operational Environmental Satellite (GOES) have been
continuously monitoring earth surface since early 1970. The frequent observations
provided by GOES sensors make them attractive for deriving information on the diurnal
land surface temperature (LST) cycle and diurnal temperature range. These parameters are
of great value for the research on the Earth's diurnal variability and climate change.
Accurate extraction of satellite-based LSTs has long been an interesting and challenging
research area in thermal remote sensing. However, derivation of LST from satellite
measurements is a difficult task because surface emitted thermal infrared radiance is
dependent on both land surface temperature and land surface emissivity (LSE), two closely
coupled variables.

Satellite LST retrievals have been conducted for over forty years from a variety of
polar-orbiting satellites and geostationary satellites. Literature relevant to satellite-based

LST retrieval techniques have been reviewed. Specifically, the evolution of two LST algorithm families, temperature and emissivity separation method (TES) and Split Window (SW) approach, have been studied in this work. This work also summarizes the LST retrieval methods especially adopted for geostationary satellites. All the existing methods could be a valuable reference to develop the LST retrieval algorithms for generating GOES LST product.

The primary objective of this study is the development of models for deriving consistent GOES LSTs with high spatial and high temporal coverage. Proper LST retrieval algorithms will be studied according to the characteristics of sensors onboard the GOES series.

A new TES approach is proposed in this study for deriving LST and LSE simultaneously by using multiple-temporal satellite observations from GOES 8 to GOES 12 series. Two split-window regression formulas are selected for this approach, and two satellite observations over the same geolocation within a certain time interval are utilized. This method is particularly applicable to geostationary satellite missions from which qualified multiple-temporal observations are available. Dual-window LST algorithm is adopted to derive LST from GOES M (12)-Q series. Instead of using conventional training method to generate optimum coefficients of the LST regression algorithms, a regression tree technique is introduced to automatically select the criteria and the boundary of the sub-ranges for generating algorithm coefficients under different conditions.

GOES measurements as well as ancillary data, including satellite and solar geometry, water vapor, cloud mask, land emissivity etc., have been collected to test the

performance of the proposed LST retrieval algorithms. In addition, in order to validate the retrieval precision, the satellite-based temperature will be compared against ground truth temperatures, which include direct skin temperature measurements from the Atmospheric Radiation Measurement program (ARM), as well as indirect measurements like surface long-wave radiation observations over six vegetated sites from the SURFace RADiation Budget (SURFRAD) Network. The validation results demonstrate that the proposed GOES LST algorithms are capable of deriving consistent surface temperatures with good retrieval precision. Consistent GOES LST retrievals with high spatial and temporal coverage are expected to better serve the detections and observations of meteorological phenomena and climate change over the land surface.

Chapter 1 Introduction

1.1   Land surface temperature and diurnal temperature changes

Land surface temperature (LST) plays a critical role in the interaction between land surface and atmosphere by controlling upward terrestrial radiation and affecting surface sensible heat and latent heat flux exchange with the atmosphere. Thus, LST, as a key parameter for the Earth's surface energy balance and exchange, is of great value to the research in the fields of climatology, hydrology, meteorology and ecology, as well as a wide range of interdisciplinary research areas (Camillo 1991; Running 1991; Schmugge, Becker et al. 1991; Running, Justice et al. 1994; Zhang, Lemeur et al. 1995).

Surface skin temperatures can be achieved from field observations, such as the First International Satellite Land Surface Climatology Project (ISLSCP) Field Experiment (FIFE) (Sellers, Hall et al. 1992), Boreal Ecosystem-Atmosphere Study (BOREAS) Experiment (Sellers, Hall et al. 1995; Sellers, Hall et al. 1997), the Atmospheric Radiation Measurement Program (ARM) Experiment (http://www.arm.gov), the MONSOON Experiment (Kustas and Goodrich 1994), the Oklahoma Mesonet Network (http://okmesonet.ocs.ou.edu), the CASES experiment (http://www.mmm.ucar.edu/cases), U.S. Climate Reference Network (USCRN, http://www.ncdc.noaa.gov/crn/) and many more field experiments. Even though LSTs from field measurements have been widely used in climate change research, the limited number of observation stations makes field

measurements less useful for the detection of global change. Moreover, weather stations are usually located in relatively densely populated regions where anthropogenic impacts may affect measurements, and thus the temperature record may not be representative of global change. Thermal infrared satellite observations, however, present an efficient and practical way of capturing temperature variability globally and continuously. Deriving accurate satellite-based LSTs has long been an interesting and challenging research area in thermal remote sensing (Lorenz 1986; Nerry, Labed et al. 1990).

A satellite-based LST product is an important input to meteorological, hydrological and ecological models. The LST product generated from Moderate Resolution Imaging Spectroradiometer (MODIS) onboard the Earth Observation System satellites (EOS) Terra and Aqua provides global land surface temperature distribution in different spatial resolutions (1km and 5km) and in different temporal resolutions (daily, 8-daily, and monthly). LST products can also be acquired from Advanced Along-Track Scanning Radiometer (AATSR) onboard ESA's Envisat Satellite in 1km spatial resolution with the accuracy of 2.5K in the daytime and 1K in the night time (Noyes, Corlett et al. 2007). These LST products from polar-orbiting satellite sensors, such as MODIS or AATSR, have the advantage of high spatial resolution, but the temporal resolution is limited to two observations per day on average.

However, surface temperature, especially land surface temperature, has a strong diurnal cycle, which cannot be captured at the temporal resolution (approximately two views per day) of polar-orbit satellites. Braganza et al. (Braganza, Karoly et al. 2004) addressed the issue that mean surface temperature alone is not as useful an indicator of

climate changing as the change in daily maximum and minimum temperatures. Trends in mean surface temperature are due to changes in either maximum or minimum temperature, or relative changes in both. The recently reported global warming over land is associated with relatively larger increases in daily minimum temperature rather than in maximum temperature (Karl, Jones et al. 1993; Kin'uyu, Ogallo et al. 1999). This means diurnal temperature range (DTR) is an important index of climate change (Karl, Kukla et al. 1984), and is susceptible to urban effects. Under these circumstances, only geostationary orbit satellites have the potential abilities to provide frequent LST observations for climatology and support the research on diurnal changes.

1.2 Geostationary Operational Environmental Satellites

Geostationary Operational Environmental Satellite (GOES) have been continuously monitoring earth surface through three generations starting from early 1970 and provided qualitative and quantitative land surface measurements. GOES series are now heading to the 4th generation. GOES-R, as a representative of the new generation of the GOES series, is scheduled to be launched in 2015. Obtaining better coverage and accuracy of surface temperatures is one of the most essential objectives for new GOES generations (Dittberner, Grid et al. 1996). Two adjacent thermal infrared bands of Advanced Baseline Imager (ABI) equipped in GOES-R, which are especially designed for LST retrieval, will be considerably improved in terms of spatial resolution (up to 2km), noise equivalent temperature (0.1K) and refresh rate (5 min). The ABI measurements with high temporal resolution over the hemisphere will be a unique data source for studies of the Earth's diurnal variability.

3

Since the design of algorithms is closely dependent on the channel settings of the sensors, the GOES series are divided into two categories in our study according to channel allocation of infrared bands. The imagers with split window (SW) channels belong to the first category, while those without SW channels are the second.

GOES 8-11 as well as the new generation GOES-R belong to the first category, which have SW channels (Schmit, Gunshor et al. 2005). The channels allocation and more designed parameters of GOES 8-11 and GOES-R are shown in Table 1-1 and Table 1-2, respectively. Imagers onboard on GOES-M (12) to GOES-Q belong to the second category, which have only one thermal window channel. The parameters of GOES M (12)-Q are shown in Table 1-3.

Table 1-1 Channels allocation of GOES 8-11

Infrared channels	Wavelength range (μm)	Central Wavelength (μm)	Range of measurement (K)	Spatial resolution (km)	Meteorological objective and maximum temperature range
4	10.20 - 11.20	10.7	4 - 320	4	Surface temperature and water vapor (space – 335 K)
5	11.50 - 12.50	12.0	4 - 320	4	Surface temperature and water vapor (space – 335 K)

Table 1-2 Channels allocation of GOES-R

Infrared channels	Wavelength range (µm)	Central Wavelength (µm)	Spatial resolution (km)	Range of measurement (K)	Sample use
14	10.8-11.6	11.2	2	233-333	Imagery, Surface temperature, clouds, rainfall
15	11.50 - 12.50	12.3	2	233-333	Total water, ash and SST

Table 1-3 Channel allocation of GOES 12 - Q

Infrared channels	Wavelength range (µm)	Range of measurement	Detector type	Spatial resolution (km)	Meteorological objective and maximum temperature range
2	3.80 - 4.00	4 - 335 K	InSb	4	Nighttime clouds (space – 340 K)
4	10.20 - 11.20	4 - 320 K	HgCdTe	4	Surface temperature and water vapor (space – 335 K)

Currently, GOES LST product is generated as a byproduct of GOES Surface and Insolation Products (GSIP). The GSIP LST product is poor in resolution with unknown accuracy. With the qualitative and quantitative archive from current and oncoming GOES missions, consistent GOES LSTs with better accuracy and high resolution are needed to meet the increasing requirements in research projects related to ecosystems, weather and climate.

1.3 Outline of the thesis

This thesis is organized as following. A review of literatures relevant to LST retrieval methods is given in Chapter 2. Methodology outline will be described in Chapter 3, followed by detailed introduction on the principle and implementation of LST retrieval algorithms adopted in this study. Chapter 4 introduces datasets which are collected to support the implementation of the proposed algorithms, including GOES measurements, ancillary data set and validation data. The results of LST retrievals are presented in Chapter 5. And a validation effort is made by comparing the retrieval LST with the ground truth temperature measurements in the last part of Chapter 5. Finally, discussions and conclusions are presented in Chapter 6 and 7, respectively.

Chapter 2 Literature Review

Due to the complexity of the land surface, the heterogeneity of LST, and the limitations of thermal remote sensors, the accuracy of retrieved LSTs may not meet some application requirements. How to increase retrieval accuracy has always been a primary objective in the thermal remote sensing community. The studies in thermal remote sensing may be briefly categorized into three areas, temperature and emissivity separation (TES), removing atmospheric effect and component temperature inversion. The objective of this study is to derive LSTs at the pixel level from GOES series data. Thus, the component temperature at the sub-pixel level will not be considered here.

An overview of LST retrieval methods from the previous-mentioned two algorithm families (temperature and emissivity separation and removing atmospheric effect) will be presented in this section. In addition, literature relevant to LST inversion from geostationary satellites especially from the GOES series will be reviewed afterwards.

2.1   LST retrieval algorithms

2.1.1 Temperature and emissivity separation

High resolution LST is usually derived from thermal infrared (TIR) satellite observations using multi-channel technique. However, accurate derivations of LST and land surface emissivity (LSE) from satellite measurements are difficult tasks mainly because they are always closely coupled. In general, surface emitted TIR radiance is

dependent on both its temperature and emissivity, which also varies with the wavelength. This is particularly true for most land surfaces where emissivities are significantly less than unity. A problem of the LST retrieval from TIR measurements cannot be solved simply by adding observations in different wavelengths, because the number of unknowns is always at least one more than the measurements (Li and Barker 1993; Li, Becker et al. 1999; Liang 2001). A single measurement with N spectral bands presents N equations but have N+1 unknowns (N spectral emissivities plus LST). Without any prior information, it is impossible to retrieve both LST and LSE simultaneously.

Therefore, temperature and emissivity separation has always been a fundamental and essential problem in temperature inversion. Several attempts have been made to solve this problem by the use of additional constraints or prior knowledge. Examples of early TES algorithms include spatial ratio method (Watson 1992a), Alpha derived emissivity (Kealy and Gabell 1990), graybody method (Barducci and Pippi 1996), maximum-minimum difference (Matsunaga 1994), reference channel method (Kahle and Rowan 1980), and normalized emissivity method (Gillespie 1985).

The temperature and emissivity separation method (Alpha emissivity method) was presented and compared with the reference channel method and the normalized emissivity method by Kealy and Hook (Kealy and Hook 1993) using multispectral thermal infrared radiance data from Thermal Infrared Multispectral Scanner (TIMS) and Advanced Spaceborne Thermal Emission Reflectance Radiometer (ASTER). They pointed out that the Alpha emissivity method showed a primary advantage in deriving LSTs from terrains with widely varying and unknown emissivities.

8

A TES algorithm was applied to generate the ASTER LST product (Gillespie, Matsunaga et al. 1998) based on thermal infrared measurements from five channels. This method consisted of four major modules: NEM module (estimating the surface temperature and subtracting reflected sky irradiance), Ratio module (Ratio algorithm), MMD module (estimating TES emissivities and temperature) and final correction for sky irradiance and bias in β.

Liang (Liang 2001) further developed an optimization procedure to constraint errors in the simultaneous determination process for the LST and the emissivities from MODIS and Advanced Spaceborne Thermal Emission and Reflection Radiometer (ASTER). Five thermal channels from ASTER and six from MODIS are utilized in this algorithm. The validation effort was carried out by comparing the LST retrievals against the ground-measured LSTs, and the results showed that the differences of 84% validation pixels were within 1.5 degree.

There are also other alternative retrieval approaches to separate temperatures and emissivities, which took advantage of measurements at different times or/and different channels to compensate for the lack information of surface emissivity, such as the two-measurement method (Watson 1992b) and the Temperature-independent spectral Indices (TISI) method (Barker and Li 1990b). Ma et al. (Ma, Wan et al. 2002) proposed an extended twp-step physical algorithm to retrieve LST, surface emissivity and atmospheric profiles simultaneously from MODIS Airborne Simulator. It is also applicable to MODIS data.

In brief, the common strategy of TES methods is to bring in prior knowledge or constraint conditions. When extracting LST with accompanying unknown parameter, emissivity, which varies with both wavelength and land cover, especially in the situation of retrieving atmospheric parameters simultaneously, it is inevitable to bring in more available information, such as special characteristics of remotely sensed data (multi-temporal measurements, multiple channel measurements etc.), and all kinds of prior knowledge (known shape of emissivity curve, the relationship between emissivity and land cover etc.).

2.1.2 Split window algorithms

The SW algorithm (McMillin 1975), which achieved great success in Sea Surface Temperature (SST) retrieval, led to a big advance in the research area of temperature retrieval and greatly extended the applications of quantitative thermal remote sensing. The SW method corrects the atmospheric effect to a great extent using a linear combination of radiances from two adjacent infrared bands. It is still successfully being used to extract sea surface temperature (SST) with the accuracy of 0.5K (Minnett 1986; Ottlé and Vidal-Madjar 1992).

However, this method has some limitations in temperature retrieval over complex land surfaces because the emissivities of land covers are not equal to 1 and vary depending on the channels. Therefore, researchers have tried many possible ways to extend this method to LST extraction. Price (Price 1984) first tried to apply an AVHRR SST split window algorithm to agricultural land and concluded that the LST could be extracted with SST SW algorithm with the accuracy of 3°. The local split window method is one of the

successful examples (Barker and Li 1990a) of extending the SST SW algorithm to land surfaces. This method requires prior knowledge of sufficiently accurate emissivities in two adjacent channels. Additionally, researchers in this area pointed out that more accurate LSTs can be derived if emissivities are given with sufficient accuracy.

Becker, Li, Sobrino, and Wan et al. are the pioneers who introduced the SW technique to land surface temperature remote sensing. The MODIS team (Wan and Dozier 1996) proposed a day/night algorithm that utilized day and night measurements from 7 bands of MODIS. Specifically, the bands at 12.91, 12.25, 11.98, 8.6, 4.70, 4.11, 3.74 microns were adopted to create a 14-equation set. The coefficients of this algorithm were determined for each sub-range separately according to the ranges of atmospheric water vapor and surface air temperature.

A number of LST SW algorithms have been developed since 1990 and widely applied to produce satellite-based LSTs (Vidal 1991; Ulivieri, Castronouvo et al. 1992; Prata 1994; Caselles, Coll et al. 1997). Even though their models are different in form, the essence of the theory are almost the same; that is to build a linear relationship between the LST and the brightness temperatures of two adjacent thermal channels, where the algorithm coefficients depend on the spectral land surface emissivities. LST SW algorithms are keeping the similar form to SST SW algorithm. Among a variety of developed LST SW algorithms from the literature, nine have been adapted as candidate LST algorithms to generate LST product for the next GOES generation (Yu, Tarpley et al. 2009a), shown in the Table 2-1. Each algorithm is composed of two parts: the base split window algorithm and path length correction (the last term in each algorithm). The base

split window algorithms are adapted from those published split window algorithms as referred in the references, while the path length term is particularly added for additional atmospheric correction.

Table 2-1 Nine candidate LST algorithms for next GOES generation*

No	Formula[#]	Reference
1	$T_s = C + (A_1 + A_2 \frac{1-\varepsilon}{\varepsilon} + A_3 \frac{\Delta\varepsilon}{\varepsilon^2})(T_{11} + T_{12})$ $+ (A_4 + A_5 \frac{1-\varepsilon}{\varepsilon} + A_6 \frac{\Delta\varepsilon}{\varepsilon^2})(T_{11} - T_{12}) + D(T_{11} - T_{12})(\sec\theta - 1)$	**(Wan and Dozier 1989) (Barker and Li 1990a)**
2	$T_s = C + A_1 \frac{T_{11}}{\varepsilon} + A_2 \frac{T_{12}}{\varepsilon} + A_3 \frac{1-\varepsilon}{\varepsilon} + D(T_{11} - T_{12})(\sec\theta - 1)$	**(Prata and Platt 1991) (Caselles, Coll et al. 1997)**
3	$T_s = C + A_1 T_{11} + A_2 (T_{11} - T_{12}) + A_3 (1 - \varepsilon_{11}) + A_4 \Delta\varepsilon$ $+ D(T_{11} - T_{12})(\sec\theta - 1)$	**(Coll and Caselles 1997)**
4	$T_s = C + A_1 T_{11} + A_2 (T_{11} - T_{12}) + A_3 \frac{1-\varepsilon}{\varepsilon} + A_4 \frac{\Delta\varepsilon}{\varepsilon^2} + D(T_{11} - T_{12})(\sec\theta - 1)$	**(Vidal 1991)**
5	$T_s = C + A_1 T_{11} + A_2 (T_{11} - T_{12}) + A_3 (T_{11} - T_{12})\varepsilon_{11}$ $+ A_4 T_{12} \Delta\varepsilon + D(T_{11} - T_{12})(\sec\theta - 1)$	**(Price 1984)**
6	$T_s = C + A_1 T_{11} + A_2 (T_{11} - T_{12}) + A_3 \varepsilon + D(T_{11} - T_{12})(\sec\theta - 1)$	**(Ulivieri and Cannizzaro 1985)**
7	$T_s = C + A_1 T_{11} + A_2 (T_{11} - T_{12}) + A_3 \varepsilon + A_4 \frac{\Delta\varepsilon}{\varepsilon}$ $+ D(T_{11} - T_{12})(\sec\theta - 1)$	**(Sobrino, Li et al. 1994)**
8	$T_s = C + A_1 T_{11} + A_2 (T_{11} - T_{12}) + A_3 (1 - \varepsilon) + A_4 \Delta\varepsilon + D(T_{11} - T_{12})(\sec\theta - 1)$	**(Ulivieri, Castronouvo et al. 1992)**
9	$T_s = C + A_1 T_{11} + A_2 (T_{11} - T_{12}) + A_3 (T_{11} - T_{12})(T_{11} - T_{12})$ $+ A_4 (1 - \varepsilon_{11}) + A_5 \Delta\varepsilon + D(T_{11} - T_{12})(\sec\theta - 1)$	**(Sobrino, Li et al. 1994)**

[#]**Note:**
1) **T_{11} and T_{11} represent the top-of-atmosphere brightness temperatures of GOES IMAGER channels 14 and 15, respectively;**
2) **$\varepsilon = (\varepsilon_{11} + \varepsilon_{12})/2$ and $\Delta\varepsilon = \varepsilon_{11} - \varepsilon_{12}$ where ε_{11} and ε_{12} are the spectral emissivity values of the land surface at GOES IMAGER channels 14 and 15, respectively;**
3) **θ is the satellite view zenith angle.**
* Source note: The creator of this table is Yunyue Yu (Yu, Tarpley et al. 2009a).

Among those LST SW models, some are empirical (Vidal 1991) or semi-empirical models(Kerr, Lagouardeb et al. 1992) which are suitable for local regions; some are physical models (Ulivieri and Cannizzaro 1985; Ottlé and Vidal-Madjar 1992; Prata 1994) based on a radiative transfer mechanism.

Since the combination of two adjacent thermal channels used in SW algorithms is proven to be able to correct atmospheric effect to a great extent, the coefficients of most LST SW algorithms depend only on the spectral emissivities rather than atmospheric conditions. And yet, the SW algorithm proposed by Prata (Prata 1994) and Sobrino et al. (Sobrino, Li et al. 1994) took both land surface emissivity and atmospheric transmittance into account. Furthermore, water vapor, regarded as the major absorbing gas in the split window bands, many researchers developed the SW models with coefficients varying with the atmospheric water vapor content (Becker and Li 1995; Francois and Ottle 1996; Coll and Caselles 1997). The problem of these kinds of algorithms is that accurate water vapor data cannot be always easily obtained and hence the error of water data itself may unavoidably lead to the LST retrieval error.

2.2   LST retrieval from Geostationary Satellites

The above mentioned studies are mostly focusing on the polar orbiting satellites. Relatively less research has been carried out to extract LST from geostationary satellites observations. However, the emphasis on the research of LST diurnal cycle has drawn scientists' attention to LST retrieval from geostationary satellites, which can provide high temporal observations. Investigations have been performed to derive LSTs from

geostationary satellites, such as the Japanese Geostationary Meteorological Satellite 5 (GMS-5) (Prata and Cechet 1999), and METEOSAT of the European Meteorological Satellite Programme (EUMETSAT) (Morcrette 1991; OLesen, Kind et al. 1995; Cresswell, Morse et al. 1999; Hay and Lennon 1999; Gottsche and Olesen 2001; Schadlich, Gottsche et al. 2001; Dash, Gottsche et al. 2002; Sun and Pinker 2007) and GOES (Sun and Pinker 2003; Sun and Pinker 2004a; Sun, Pinker et al. 2004b). All LST retrieval studies for either polar-orbiting satellites or geostationary satellites are of significant reference value in the development of the GOES LST retrieval algorithms.

GOES series have been operated by National Oceanic and Atmospheric Administration (NOAA) for more than 35 years. The current LST product of GOES series is produced from Sounder sensor (Ma, Schmit et al. 1999). The temperature and water vapor profiles were achieved through the inverse solution of the nonlinear radiative transfer equation. However, the intermediate product from Sounder radiance observations is poor in resolution and with unknown accuracy.

The performance of Imagers has been improved since the second generation of GOES series were launched in April 1994. Many investigators have studied operational LST algorithms for GOES Imagers (Hayden 1988; Hayden, Wade et al. 1996; Sun and Pinker 2003; Sun and Pinker 2004a).

Faysash and Smith (Faysash and Smith 1999) addressed a combined land surface temperature-emissivity retrieval algorithm from two radiance measurements acquired at two different times of GOES-8. An optimization scheme was adopted to solve the system of equations. The validation showed that the biases between the retrieved LSTs and surface

14

measurements in the Australian, FIFE, and ARM CART study areas are approximately 0.088°, 1.78°, and 1.48°, respectively.

In the era of GOES M-Q, the LST SW algorithms are greatly limited due to the lack of SW channels. Under this constraint, a dual-window method and an approach utilizing total precipitable water were presented by Sun and Pinker (Sun, Pinker et al. 2004b) for deriving LST from the GOES M-Q. This method is proven to have less atmospheric attenuation than the split window channels.

For the next generation of the GOES series, a LST product is expected to be generated independently with more accuracy and higher resolution, which is capable of estimating the diurnal cycle and DTR, as well as supporting the research projects in the field of meteorology, climatology and ecology. Yu et al. (Yu, Tarpley et al. 2009a) investigated the performance of nine SW LST algorithms to generate GOES-R LST product , in which the surface emissivities at the two TIR channels can be obtained as priors. The analysis of accuracy and sensitivity of those retrieval algorithms showed that even though most of the LST algorithms could meet the GOES-R RMD requirement (less than 2.5K), the emissivity uncertainty significantly impacted the retrieval accuracy. Recently, a similar TES procedure has been applied to GOES R data for producing land surface emissivities from its Advanced Baseline Imager (ABI). A Simplified method was briefly described for extracting LSTs at two time stamps and emissivities at two channels from the ABI data onboard the future GOES-R (Yu, Xu et al. 2009)

2.3   Problems in LST retrieval methods

As mentioned in section 2.1, a variety of LST algorithms have been developed for years and can be adapted for extracting LSTs from GOES satellites, including both GOES-W and GOES-E. In order to choose reliable LST retrieval algorithms to generate consistent GOES LST values, the problems in the existing LST algorithms should be carefully analyzed and improvement may be made when necessary.

2.3.1 Problems in TES algorithms

For the TES problem, a set of multi-spectral thermal measurements in N bands can create N equations with N+1 unknowns, N spectral emissivities and LST. In order to deal with this so-called ill-posed inversion problem, a variety of approaches have been tried to compensate for the lack of information. Most of the TES methods for simultaneous retrievals of LST and LSE depend on a well-determined or over-determined matrix problem which is built on a multiple-channel dataset from the satellite infrared radiometer or imager and spectral radiative transfer equations (Peres and DaCamara 2006). An atmospheric profile that is usually obtained through a microwave sounder is required in solving the radiative transfer equations, which is usually in coarser spatial resolution than the thermal infrared data. The solution of the matrix problem may be unreliable as the method is known to be sensitive to noise in the input data (Peres and DaCamara 2004; Peres and DaCamara 2006). Moreover, intensive numerical computation time is required for processing the radiative transfer equations and for solving the matrix problem.

Instead of applying the radiative transfer model and the atmospheric profiles for building up the matrix inversion problem, a simplified TES method based on two satellite

observations will be presented in this study to derive LSTs and LSE simultaneously. The new TES algorithm is particularly applicable to GOES 8-11 missions in which qualified multiple-temporal observations in split window channels can be obtained. This method also shows promise for application to the new generation of GOES series.

2.3.2 Problems in traditional coefficients training

For most of the LST regression algorithms, the optimum coefficients have been determined by separating the ranges of parameters, such as atmospheric water vapor, boundary temperature and so on. The selection criteria and the boundary of the sub-ranges were always made manually, mostly based on experience.

Take the generalized split-window (GSW) algorithm as an example. Wan and Dozier (Wan and Dozier 1996) extended the local SW algorithm proposed by Becker and Li (Barker and Li 1990a) to a GSW algorithm by making the coefficients varying according to different conditions.

$$T_s = C + \left(A_1 + A_2 \frac{1-\varepsilon}{\varepsilon} + A_3 \frac{\Delta\varepsilon}{\varepsilon^2}\right)(T_{11} + T_{12}) + \left(A_4 + A_5 \frac{1-\varepsilon}{\varepsilon} + A_6 \frac{\Delta\varepsilon}{\varepsilon^2}\right)(T_{11} - T_{12})$$

$$+D(T_{11} - T_{12})(\sec\theta - 1) \qquad\qquad (Eq. 2\text{-}1)$$

Where T_{11} and T_{12} represent the top-of-atmosphere brightness temperature at around 11 and 12 microns, respectively; $\varepsilon = \frac{\varepsilon_{11}+\varepsilon_{12}}{2}$ and $\Delta\varepsilon = \varepsilon_{11} - \varepsilon_{12}$; ε_{11}, ε_{12} are the emissivities at the two channels; θ is the satellite view zenith angle; $A_i(i = 1,2,...6)$ and C are algorithm coefficients that depend on the spectral emissivities only.

In this GSW algorithm, Wan and Dozier made the coefficients in Becker and Li's SW algorithm changing according to some suggested initial guess values, or some kind of

bins of 9 viewing angles (Cosine values of these angles are 0.415059, 0.445869, 0.475084, 0.529560, 0.626080, 0.713005, 0.781367, 0.966438, and 0.998631), 7 surface air temperatures (273, 281, 289, 295, 300, 305, 310, units:K), and 11 atmospheric column water vapor amount (0.5, 1.0, 1.5, 2.0, 2.5, 3.0, 3.5, 4.0, 4.5, 5.0, 5.5, units:cm/km). How to determine these threshold values for different surface and atmospheric conditions may be the tricky part and mostly predefined based on experience. Regression Tree algorithm can allow us to integrate all the possible candidate predictors, such as GOES brightness temperatures and emissivities at the window channels, solar and satellite geometry, atmospheric column water or total precipitable water etc., and at the same time, it can determine the threshold values for different conditions, and give accuracy estimates.

2.3.3 Other problems

LST retrieval algorithms are extremely dependent on the channel settings of the sensors. GOES 8-11 and GOES-R have two split windows bands, while GOES M-Q series have not. GOES LST retrieval algorithms will be designed under different principles according to the two different sets of channel setting in GOES sensors. Moreover, there is very poor validation for current GOES LSTs. Validation methodology of GOES LST retrievals should be one of the concerns in this study.

2.4 Summary of literature review

Literatures have shown that consistent LST data set with high spatial and temporal coverage are in great demand to better serve the detections and observations of meteorological phenomena over the land surface. The unique characteristic of geostationary satellite data with hourly temporal resolution is of tremendous value for the

studies of the Earth's diurnal variability. How to develop proper LST retrieval algorithms to generate consistent LST products for GOES series according to the characteristics of onboard sensors becomes the primary objective of this study.

After reviewing the literatures relevant to pixel-level LST retrieval methods, the major problems in deriving LST from thermal remote sensing observations have been analyzed. In brief, the uncertainty in complex matrix problem in current TES algorithms is still a great concern, and the generation of optimum coefficients in LST regression algorithm is also a challenging work. Furthermore, poor validation of current GOES LST product greatly limited its applications.

Improvement will be made in this work for the above mentioned aspects. Specifically, to avoid solving complex matrix based on radiative transfer model and atmospheric profiles, a simplified TES method will be proposed to derive LSTs and LSE simultaneously by utilization of multiple-temporal thermal observations. Secondly, decision tree will be introduced to automatically derive algorithm coefficients and threshold values. Furthermore, the performance of satellite-based LSTs will be validated against the ground truth of skin temperature observations, including direct skin temperature measurement such as LST observations from the Atmospheric Radiation Measurement program (ARM), MESONET and U.S. Climate Reference Network (USCRN), as well as indirect measurements like surface long-wave radiation observations over eight vegetated sites from the SURFace RADiation Budget Network (SURFRAD).

19

Chapter 3 Methodology

3.1 Overview

The methodology outline of this study is summarized in the flow chart in Figure 3-1. The process is started by extracting and pre-processing measurements from GOES imager sensor. The process is then divided into two branches according to the two different types of GOES sensors (with/without SW bands). The new TES approach will be applied to the data from GOES Imagers with SW bands, whereas the dual-window LST retrieval approach will be adopted for GOES sensors without SW bands. The principles and procedures of these two algorithms will be described in detail in section 3.3 and 3.4, respectively. The ancillary datasets are required for both algorithms, including satellite/solar geometry, cloud mask, monthly emissivity, total water vapor, and land/ocean mask. Following that, the satellite-based LSTs will be compared with in-situ skin temperature measurements to validate the performances of the retrieval models. The ground-based measurements include skin temperature measurements from ARM, MESONET and CRN, as well as long-wave radiation observations over eight vegetated sites from SURFRAD, which are converted to temperatures before comparison with LST retrievals.
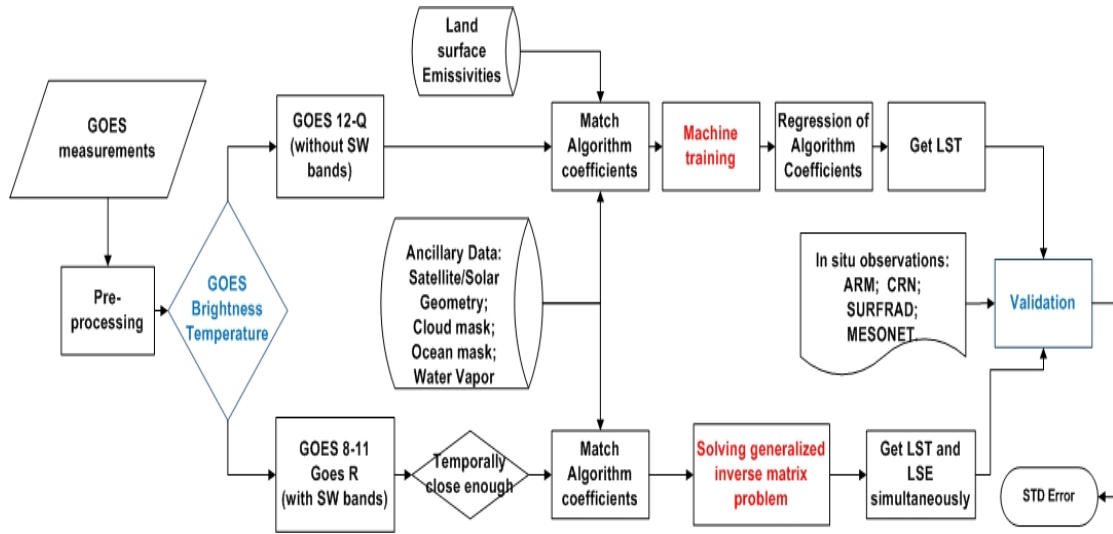
Figure 3-1. Methodology outline of the study

3.2 Data pre-processing

3.2.1 Data calibration

The original GOES data downloaded from the CLASS are in the format of GVAR (GOES variable format) which are scaled radiances in 10-bit digits. The GVAR data need to be converted to brightness temperatures in several steps (Weinreb, Jamieson et al. 1997). Firstly, the 10-bit GVAR value should be converted to scene radiance by a linear conversion equation. The radiance is then converted to effective brightness temperature through the inverse of the Planck function. Finally, the effective temperature is converted to a top-of-atmosphere brightness temperature.

1. Conversion of Imager GVAR Count to Scene Radiance

Original Imager GVAR Count needs to be converted to scene radiance with the formula:

$$R = (X - b)/m \qquad\qquad \text{Eq. 3-1}$$

where R is radiance (unit: $nw \cdot m^{-2} \cdot sr^{-1} \cdot cm^{-1}$) and X is the GVAR count value. Parameters of b and m vary with the sensors. The b and m values for GOES 8-O are shown in Table 3-1.

Table 3-1 GOES-8 through -O Imager Scaling Coefficients

GOES	Channel	m	b
GOES-8-11	2	227.3889	68.2167
GOES-8-11	4	5.2285	15.6854
GOES-8-11	5	5.0273	15.3332
GOES-12-O	2	227.3889	68.2167
GOES-12-O	4	5.2285	15.6854

Data source:

http://www.oso.noaa.gov/goes/goes-calibration/gvar-conversion.htm

2. Conversion of Scene Radiance to Temperature

Before transferred to temperature, scene radiance needs to be converted to effective temperature T_{eff} (K) by the inverse of Planck function:

$$T_{eff} = \frac{c_2 * n}{\ln[1 + (c_1 * n^3)/R]} \qquad \text{Eq. 3-2}$$

The constants c_1 and c_2 are invariant for GOES sensors, whereas n value depends on the channels. Further, the effective temperature can be converted to actual temperature T (K) by the following relationship:

$$T = a + b * T_{eff} \qquad \text{Eq. 3-3}$$

The constants a, b and n in the above formulas vary with the channels and sensors, which are specifically given in Table 3-2.

Table 3-2 GOES-8 through -O Imager Coefficients

GOES	Channel	n	a	b
GOES-8	2	2556.71	-0.578526	1.001512
GOES-8	4	934.30	-0.322585	1.001271
GOES-8	5	837.06	-0.422571	1.001170
GOES-9	2	2555.18	-0.579908	1.000942
GOES-9	4	934.59	-0.384798	1.001293
GOES-9	5	834.02	-0.302995	1.000941
GOES-10	2	2552.9845	-0.60584483	1.0011017
GOES-10	4	936.10260	-0.27128884	1.0009674
GOES-10	5	830.88473	-0.26505411	1.0009087
GOES-11	2	2562.07	-0.644790	1.000775
GOES-11	4	931.76	-0.306809	1.001274
GOES-11	5	833.67	-0.333216	1.001000
GOES-12	2	2562.45	-0.650731	1.001520
GOES-12	4	933.21	-0.360331	1.001306
GOES-13	2	2561.74	-1.437204	1.002562
GOES-13	4	937.23	-0.386043	1.001298
GOES-14	2	2572.47	-1.530285	1.002507
GOES-14	4	934.04	-0.263369	1.001176

Data source: http://www.oso.noaa.gov/goes/goes-calibration/gvar-conversion.htm

3.2.2 Navigation or geolocation

As mentioned in section 3.2.1, the GOES observations are formatted in GVAR. GVAR provides two types of information, which are supplemental data and sensor data (NOAA/NESDIS 1998). Navigation (NAV) block, one of three major blocks (Directory

block, Navigation block and Calibration block) in the sensor data, provides orbit and attitude (O&A) coefficient set, which can be used for earth location determination. Parameters concerning the sensing geometry (interior orientation) and position/attitude of the sensing (exterior orientation) are recorded in NAV block, more specifically, information like satellite orbit position, the compensation parameters for spacecraft disturbance, spacecraft attitude angles (roll, pitch and yaw), as well as epoch date and time.

Given the relationship between instrument-related coordinate systems and geographic coordinates, the transformations between pixel coordinates (i, j) and earth-fixed coordinated can be conducted based on the principles of photogrammetry. The transformation process consists of a series of multiplication of rotation matrices, which are set up according to the interior orientation, exterior orientation, imaging time and attitude misalignment angles etc.

3.2.3 Compute satellite and solar geometry

The radiance acquired by sensors is affected by the variability in solar and satellite geometry. Therefore, the solar zenith angel for each pixel will be calculated according to the longitude, latitude, Julian day and GMT time. Also a satellite zenith angle or satellite viewing angle will be computed according to the orbit height, spatial resolution etc.

3.3   The new TES method for GOES 8-11/R

3.3.1 Mathematic description

Wan et al. (Wan, Member of IEEE et al. 1997) first developed a two-measurement algorithm for deriving LST and LSE simultaneously using polar orbiting satellite measurements of infrared channels. The basic assumption of this method is that during the

two-time measurements (i.e., day and night for the polar orbiting satellite), the surface emissivities of infrared channels remain the same. Limitations of this method have been discussed in the LST community. Firstly, since the two-measurement method requires the measurements from the day and night observations, cloud-free condition for the two measurements greatly limited the retrieval availability. Secondly, the algorithm is much affected by the assumption that emissivity of each infrared channel does not vary from daytime to nighttime. In addition, the algorithm relies on atmospheric profile, which is obtained in a coarse resolution and may introduce significant errors, for solving the radiative transfer equations.

However, it is a promising attempt to extend this two-measurement approach to extract LST from geostationary-orbiting satellite observations. High temporal refresh rate of the GOES satellite observation not only ensures significantly large number of the cloud-free data pairs for the retrieval availability, but also enriches the assumption that the surface emissivity remains the same in a short temporal interval. If dependency on the radiative transfer process can be released from the two-measurement method, which also implies that the real-time atmospheric profile information is not needed, it would be ideal applying this approach to the GOES satellite mission. To reach this goal, a basic principle of the new TES method is briefly introduced here.

Assuming that there are two established algorithms, $F()$ and $G()$, for deriving the satellite LST (T_s) for a given pixel. In our case, $F()$ and $G()$ represent two linear SW LST algorithms. When applying these two algorithms to two measurements at two different times at t_1 and t_2, we have:

$$T_{s,t_i} = f_0\big(T_{11,t_i}, T_{12,t_i}, \theta_{t_i}\big) + f_1\big(T_{11,t_i}, T_{12,t_i}, \theta_{t_i}\big)X_1(\varepsilon_{11}, \varepsilon_{12})$$

$$+ f_2\big(T_{11,t_i}, T_{12,t_i}, \theta_{t_i}\big)X_2(\varepsilon_{11}, \varepsilon_{12})$$

$$T_{s,t_i} = g_0\big(T_{11,t_i}, T_{12,t_i}, \theta_{t_i}\big) + g_1\big(T_{11,t_i}, T_{12,t_i}, \theta_{t_i}\big)X_1(\varepsilon_{11}, \varepsilon_{12})$$

$$+ g_2\big(T_{11,t_i}, T_{12,t_i}, \theta_{t_i}\big)X_2(\varepsilon_{11}, \varepsilon_{12})$$

$$i = 1, 2. \hspace{3cm} \text{Eq. 3-4}$$

where T_{11,t_i} and T_{12,t_i}, are the brightness temperatures measured by the satellite sensors around 11 μm and 12 μm at time t_i; ε_{11}, ε_{12} are the emissivities at the two channels; θ_{t_i} is the satellite view zenith angle at time t_i, and θ_{t_1} and θ_{t_2} are the same for the geostationary satellite sensor observing a certain ground area; functions $f_j()$ and $f_j()$ (j=0, 1, 2) are certain brightness temperature dependencies in the two SW LST algorithms F() and G(), respectively; $X_1(\varepsilon_{11}, \varepsilon_{12})$ and $X_2(\varepsilon_{11}, \varepsilon_{12})$ are fixed relationships derived from ε_{11} and ε_{12}, such as $X_1(\varepsilon_{11}, \varepsilon_{12}) = (\varepsilon_{11} + \varepsilon_{12})/2$.

These independent equations can be posed as a linear algebra problem in the matrix form:

$$aX = b \hspace{3cm} \text{Eq. 3-5}$$

where $X = (T_{s,t_1} \; T_{s,t_2} \; X_1 \; X_2)$. To be more specific,

$$
\begin{bmatrix}
1 & 0 & -f_1\big(T_{11,t_1}, T_{12,t_1}, \theta\big) & -f_2\big(T_{11,t_1}, T_{12,t_1}, \theta\big) \\
1 & 0 & -g_1\big(T_{11,t_1}, T_{12,t_1}, \theta\big) & -g_2\big(T_{11,t_1}, T_{12,t_1}, \theta\big) \\
0 & 1 & -f_1\big(T_{11,t_2}, T_{12,t_2}, \theta\big) & -f_2\big(T_{11,t_1}, T_{12,t_2}, \theta\big) \\
0 & 1 & -g_1\big(T_{11,t_2}, T_{12,t_2}, \theta\big) & -g_2\big(T_{11,t_1}, T_{12,t_2}, \theta\big)
\end{bmatrix}
\begin{bmatrix}
T_{s,t_1} \\
T_{s,t_2} \\
X_1 \\
X_2
\end{bmatrix}
=
\begin{bmatrix}
f_0\big(T_{11,t_1}, T_{12,t_1}, \theta\big) \\
g_0\big(T_{11,t_1}, T_{12,t_1}, \theta\big) \\
f_0\big(T_{11,t_2}, T_{12,t_2}, \theta\big) \\
g_0\big(T_{11,t_2}, T_{12,t_2}, \theta\big)
\end{bmatrix}
$$

There are four unknowns ($T_{s,t_1}, T_{s,t_2}, \varepsilon_{11}$ and ε_{12}) in the matrix X, which can be solved uniquely if the equations are not singularly posed. Thus, the algorithms F() and G() must be independent, and the two measurement (T_{11,t_1}, T_{12,t_1}), (T_{11,t_2}, T_{12,t_2}) must be

significantly different. To avoid singularity in this approach, temperatures at the two selected times should have significant difference, while the emissivities at the two-measurement times should remain the same.

In our application, two SW LST algorithms are utilized as these established linear regression formulas, f() and g(). Assuming f() represents the SW LST algorithm developed by Wan and Dozier in 1996 (Wan and Dozier 1996), which is mathematically written as:

$$T_s = C + \left(A_1 + A_2 \frac{1-\varepsilon}{\varepsilon} + A_3 \frac{\Delta\varepsilon}{\varepsilon^2}\right)(T_{11} + T_{12}) +$$

$$\left(A_4 + A_5 \frac{1-\varepsilon}{\varepsilon} + A_6 \frac{\Delta\varepsilon}{\varepsilon^2}\right)(T_{11} - T_{12}) +$$

$$D(T_{11} - T_{12})(\sec\theta - 1). \qquad \text{Eq. 3-6}$$

Again, in Eq. 3-6, T_{11} and T_{12} represent the top-of-atmosphere brightness temperatures of the TIR channels at 11 μm and 12 μm, respectively; ε_{11} and ε_{12} are the spectral emissivity values of the land surface at ABI channels 14 and 15, respectively; $\varepsilon = (\varepsilon_{11} + \varepsilon_{12})/2$ and $\Delta\varepsilon = \varepsilon_{11} - \varepsilon_{12}$; a path-length correction term $(T_{11} - T_{12})(\sec\theta - 1)$ is used to minimize the water vapor effects with increasing view angle of the satellite, which cannot be ignored to geostationary orbit satellites with high orbit altitude (Yu, Privette et al. 2008). Eq. 3-6 can be rearranged in this method, in terms of the unknown matrix X, which is:

$$T_s = [C + A_1(T_{11} + T_{12}) - A_2(T_{11} + T_{12}) + A_4(T_{11} - T_{12}) - A_5(T_{11} - T_{12}) + D(T_{11} - T_{12})(\sec\theta - 1)] + [A_2(T_{11} + T_{12}) + A_5(T_{11} - T_{12})]X_1$$

$$+[A_3(T_{11} + T_{12}) + A_5(T_{11} - T_{12})]X_2 \qquad \text{Eq. 3-7}$$

Similarly, if g() stands for the SW LST algorithm developed by Vidal in 1991 (Vidal 1991), which is written as:

$$T_s = C + A_1 T_{11} + A_2(T_{11} - T_{12}) + A_3 \frac{1-\varepsilon}{\varepsilon} + A_4 \frac{\Delta\varepsilon}{\varepsilon^2} + D(T_{11} - T_{12})(\sec\theta - 1) \qquad \text{Eq. 3-8}$$

Then, the formula will be adapted in the new method as:

$$T_s = C + A_1 T_{11} + A_2(T_{11} - T_{12}) - A_3 + D(T_{11} - T_{12})(\sec\theta - 1)$$
$$+ A_3 X_1 + A_4 X_2 \qquad \text{Eq. 3-9}$$

where X_1 and X_2 denote $1/\varepsilon$ and $\frac{\Delta\varepsilon}{\varepsilon^2}$, respectively. In our application, all the SW LST algorithms selected for the new TES method are stratified atmospheric conditions (dry/moist) and illumination conditions (daytime/nighttime).

Similar to the combination of Wan and Dozier and Vidal's algorithms (Combination A), another combination of two algorithms (Coll and Valor, 1997 and Price, 1984; Combination B) is derived and implemented for comparison. Among currently available SW LST algorithms (Price 1984; Ulivieri and Cannizzaro 1985; Barker and Li 1990a; Vidal 1991; Ulivieri, Castronouvo et al. 1992; Coll, Caselles et al. 1994; Prata 1994; Sobrino, Li et al. 1994; Wan and Dozier 1996; Caselles, Coll et al. 1997), some other combinations are also feasible to the this method(e.g., the combination of Ulivieri's (Ulivieri and Cannizzaro 1985) and Sobrino's (Sobrino, Li et al. 1994)). However, some are not appropriate for this method because of potential singularity problem or computational complexity.

3.3.2 Implementation

The main process procedures of the new TES method are given in Figure 3-2. The essential steps for the implementation of the new TES method include:

1. Read in parameters pertinent to the measurements such as observing date, time interval and so on;

2. Read in the specific matrix coefficients of the two algorithms needed to be combined;

3. Read in the satellite data along with the relevant attributes of the observation such as satellite zenith angle, cloud cover, water content and so on;

4. Calculate the LST and emissivity pixel by pixel

   a) Read in 2-measurement data;

   b) Ensure the two measurements are close enough (intervals less than three hours);

   c) Ensure the observation is cloud-free;

   d) Read in the matched algorithm coefficients according to the atmospheric condition: Daytime (solar zenith < 85 deg) or nighttime, dry (atmospheric total column water vapor <=2.0 g/cm2) or moist atmospheric conditions;

   e) Calculate the matrix A and matrix B;

   f) Calculate the solution vector X by solving generalized inverse matrix using Singular Value Decomposition method.

5. Output the results of LST at two adjacent times and emissivities at two channels pixel by pixel.
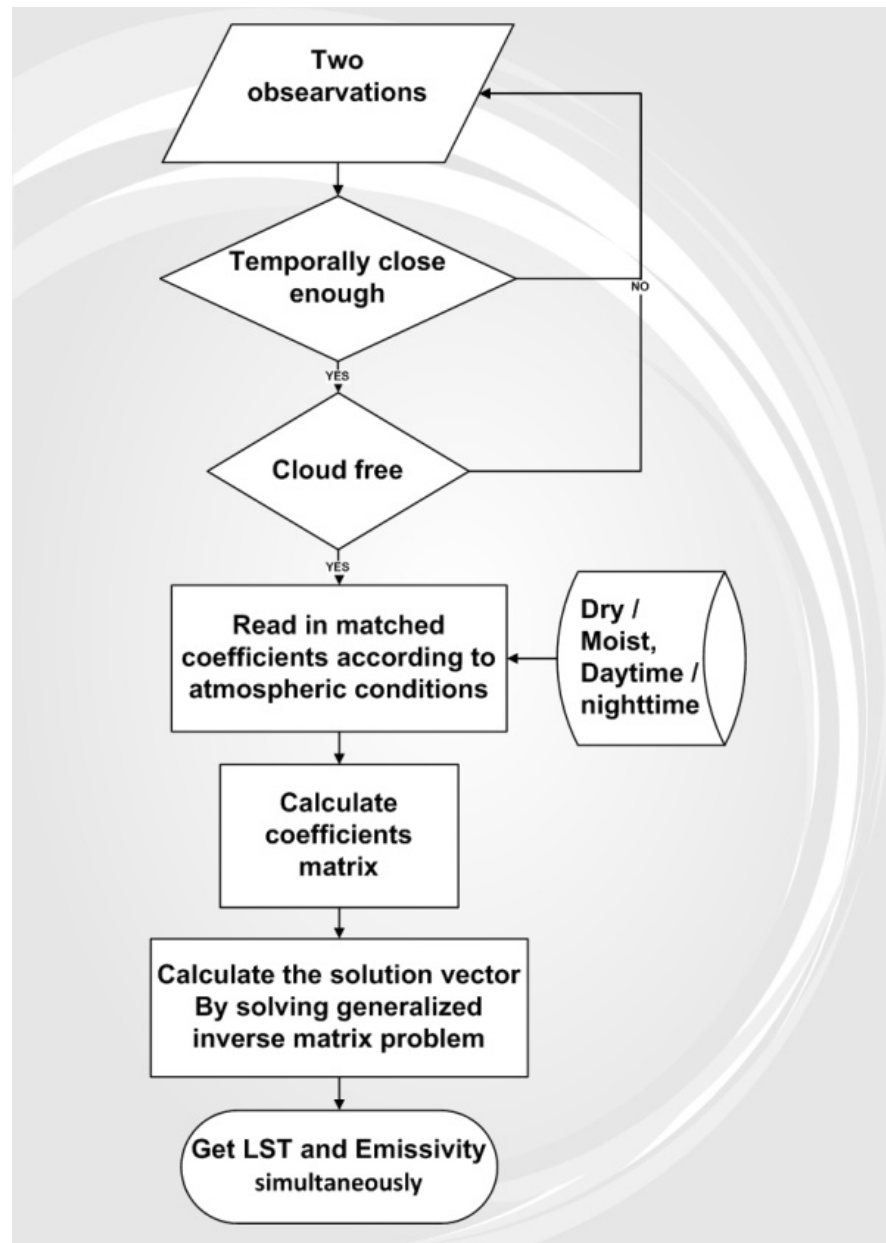
Figure 3-2 Flow chart of the new TES method for GOES 8-11/R

3.4 Dual-window algorithm for GOES M-Q

3.4.1 Mathematic description

Instead of two TIR channels in GOES8-11series, sensors onboard GOES M (12)-Q series have only one thermal window centered at 11.0 microns. Therefore, the traditional split window LST algorithms cannot be applied to extract LST from GOES M (12)-Q. In this case, Sun and Pinker (Sun, Pinker et al. 2004b) proposed two algorithms based on radiative transfer theory to derive LST from GOES M(12)-Q. One is the dual-window algorithm by introducing the middle infrared channel (centered at 3.9 microns) to improve the atmospheric correction. Mathematically the models for day time and night time are expressed as:

$$\text{Daytime: LST} = a_0 + a_1 T_{11} + a_2 (T_{11} - T_{3.9}) + a_3 (T_{11} - T_{3.9})^2$$

$$+ a_4 (\sec\theta - 1) + a_5 T_{3.9} \cos\theta_s + a_6 (1 - \varepsilon) + a_7 \Delta\varepsilon$$

$$\text{Nighttime: LST} = a_0 + a_1 T_{11} + a_2 (T_{11} - T_{3.9}) + a_3 (T_{11} - T_{3.9})^2$$

$$+ a_4 (\sec\theta - 1) + a_5 (1 - \varepsilon) + a_6 \Delta\varepsilon \qquad \text{Eq. 3-10}$$

where θ is the satellite zenith angle, θ_s, is the solar zenith angle, and $\varepsilon = (\varepsilon_{11} + \varepsilon_{3.9})/2$, and $\Delta\varepsilon = \varepsilon_{11} - \varepsilon_{3.9}$.

The other model utilized total precipitable water (TPW) as ancillary input data, which can be presented as:

$$\text{LST} = a_0 + a_1 T_{11} + a_2 W \sec\theta + a_3 (1 - \varepsilon_{11}) \qquad \text{Eq. 3-11}$$

These two models are derived from radiative transfer theory and formed into a regression-based relationship. These two algorithms will be adopted in this study to derive LST from GOES M (12)-Q. In order to obtain the algorithm coefficients, machine learning,

31

as a substitution for the traditional regression, will be utilized to train the coefficients from the matched observations. Two kinds of regression trees (Witten and Frank 2005) have been adopted in this study. Compared with traditional regression, in which the conditional judgments are made manually mostly based on experience, machine training presents a more rigorous and repeatable method for generating rules based on the analysis of the samples themselves.

3.4.2 Implementation

The process of implementation of dual-window algorithm for GOES M-Q series is presented in Figure 3-3, which includes:

1. Read in GOES imager sensor datasets in McIDAS AREA format;

2. Calculate pixel geolocation, solar-target-sensor geometry;

3. Perform calibration;

4. Calculate the LST retrieval pixel by pixel

   a) Ensure the land type is land type (algorithm applied to non-ocean pixel only);

   b) Ensure the observation is cloud-free;

   c) Read in the matched algorithm coefficients, which are stratified according to the atmospheric condition: Daytime (solar zenith < 85 deg) or nighttime, dry (atmospheric total column water vapor <=2.0 g/cm2) or moist atmospheric conditions;

   d) Calculate pixel LST retrieval

5. Output the results of LST at two adjacent times and emissivities at two channels pixel by pixel.
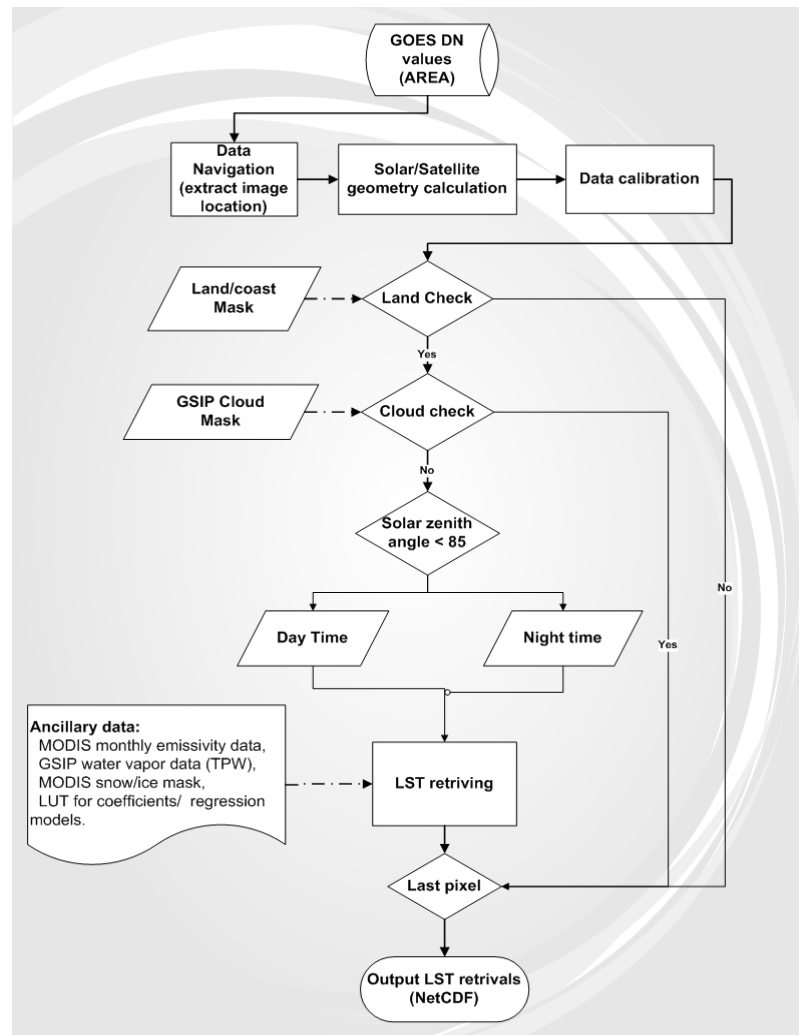
Figure 3-3 Flow chart of the new TES method for GOES M-Q

3.5 Validation

The in-situ LST measurements will be collocated with the retrieved GOES LSTs at the same time over the same location. Spatial and temporal re-samplings are used when necessary. The ground-based LST measurements available include direct skin temperature measurements such as ARM, MESONET and CRN, as well as indirect measurement like surface long-wave radiation observations from SURFRAD.

The SURFRAD observed surface long-wave radiation (upwelling and downwelling radiative fluxes) by a precise infrared radiometer (PIR), in the spectral range from 3μm to 50μm, can be converted to surface skin temperature by the following equation:

$$T_s = \left[\frac{F^{\uparrow} - (1-\varepsilon)F^{\downarrow}}{\varepsilon\sigma}\right]^{1/4} \qquad \text{Eq. 3-12}$$

Where ε is the surface broadband emissivity, σ is the Stefan-Boltzmann constant.

Chapter 4 Data

GOES measurements as well as ancillary data (satellite and solar geometry, water vapor, daily or monthly land emissivity, land/sea mask et al.) are utilized as input data to the GOES LST retrieval models.

4.1   GOES measurements

GOES Imager data are mainly available from the Comprehensive Large Array-data Stewardship System (CLASS) of National Oceanic and Atmospheric Administration (NOAA) (available online at http://www.nsof.class.noaa.gov/saa/products/welcome). Details of the availability of GOES data are shown in Table 4-1.

Table 4-1 Availability of GOES data in CLASS

Satellite	Start Date	End Date	Location	Longitude
GOES-8	09/01/94	04/01/03	East	75°W
GOES-9	01/09/96	07/21/98	West	135°W
GOES-9++	04/23/03	07/13/04	GMS-5	155°E
GOES-10	07/21/98	06/21/06	West	135°W
GOES-10	06/27/06	Present	South America	60°W
GOES-11	06/21/06	Present	West	104°W, 135°W
GOES-12	04/01/03	Present	East	75°W
GOES-13	05/24/06	Present	Central	105°W
GOES-14	06/27/09	Present	Central	89.5°W

4.2   Ground-based measurements

1. ARM: The Near-Surface Observation Data Set-1997 (NESOB-97) from the ARM provides continuous temperature measurements with a thirty-minute interval from the Cloud and Radiation Testbed (ARM/CART) site, which is located at Lamont, Oklahoma (36.607N, -97.489W).

2. MESONET: Skin temperature observations from the Oklahoma Mesonet network.

3. USCRN: Skin temperatures are measured by Apogee Instruments IRTS-P infrared temperature sensor with 5-min interval over 114 stations distributed in the continental United States.

4. SURFRAD: It continuously monitors components of the surface radiation budget, which is then converted to skin temperatures.

4.3   Collected data and data sources

The summary of the collected data and its sources are shown in Table 4-2.

Table 4-2 Collected data and data sources

Parameter	Date	Format	Resolution	Volume	Location
GOES-8[1,2]	April, July, Dec. 1997	raw	0.5°	15.6GB	U.S.
GOES-12[2]	Jan., April, July, Dec. 2004	NetCDF	4km	25.64GB	U.S.
Emissivity [1,3]	Jan., April, July, Dec. 2004	HDF	0.05°	532.7MB	Global
Cloud mask[1]	April, July, Dec. 1997 / Jan., April, July, Dec. 2004	raw	0.5°	1.7GB	U.S.
Snow mask[4]	April, July, Dec. 1997 / Jan., April, July, Dec. 2004	HDF	0.05°	5.25GB	Global
Water vapor[1]	April, July, Dec. 1997 / Jan., April, July, Dec. 2004	raw	0.5°	1.7GB	U.S.
Satellite/solar geometry[1]	April, July, Dec. 1997 / Jan., April, July, Dec. 2004	raw	0.5°	1.7GB	U.S.
ARM[5]	1997, 2004	TXT	- -	1.59MB	U.S.
MESONET[6]	1997, 2004	TXT	- -	480MB	Oklahoma
CRN[7]	1997, 2004	TXT	- -	18.3MB	U.S.
SURFRAD[8]	1997, 2004	TXT	- -	193.2MB	U.S.

Data source:
1. NOAA GOES Surface and Insolation Products (GSIP)
2. Comprehensive Large Array-data Stewardship System (CLASS), National Oceanic and Atmospheric Administration (NOAA)
3. National Aeronautics and Space Administration (NASA), Warehouse Inventory Search Tool (WIST). https://wist.echo.nasa.gov/api/
4. National snow and ice data center (NSIDC)
5. Atmospheric Radiation Measurement (ARM) Climate Research Facility. http://www.arm.gov/
6. Mesonet, Oklahoma. http://www.mesonet.org/
7. The U.S. Climate Reference Network (USCRN). ftp://ftp.ncdc.noaa.gov/pub/data/uscrn/products/hourly02/
8. Earth System Research Laboratory, NOAA. ftp://ftp.srrb.noaa.gov/pub/data/surfrad/

Chapter 5 Results of LST retrievals and validation

5.1   Calibration results

As introduced in section 3.2, calibration will be carried out in pre-process procedures. The GOES measurements before and after calibration are shown in Figure 5-1 and Figure 5-2. The scale bars demonstrate the conversion from GVAR value to brightness temperature. The GVAR data ranges from 0 to 8758, while calibrated image ranges from 205K to 315K.
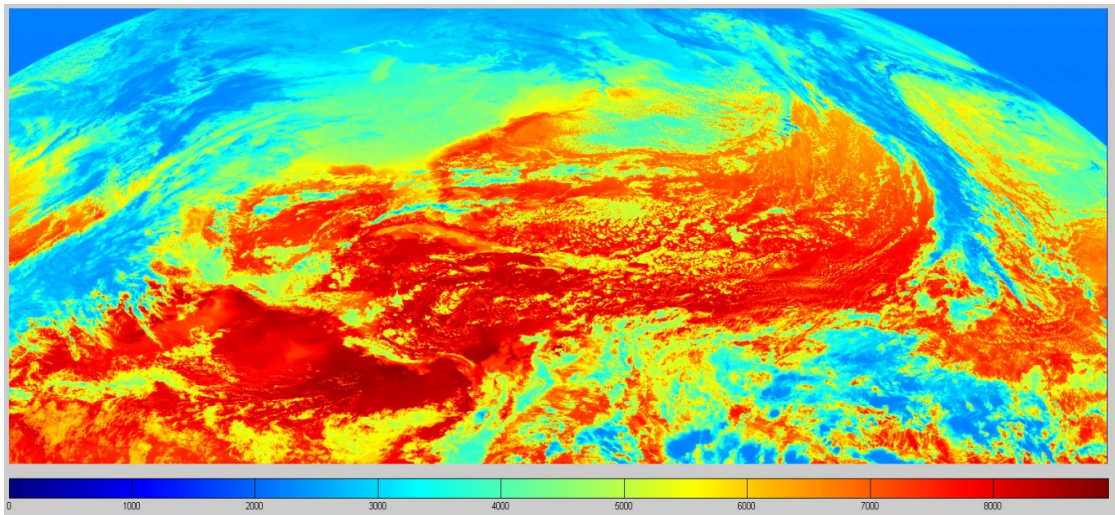
Figure 5-1 GOES measurement before calibration
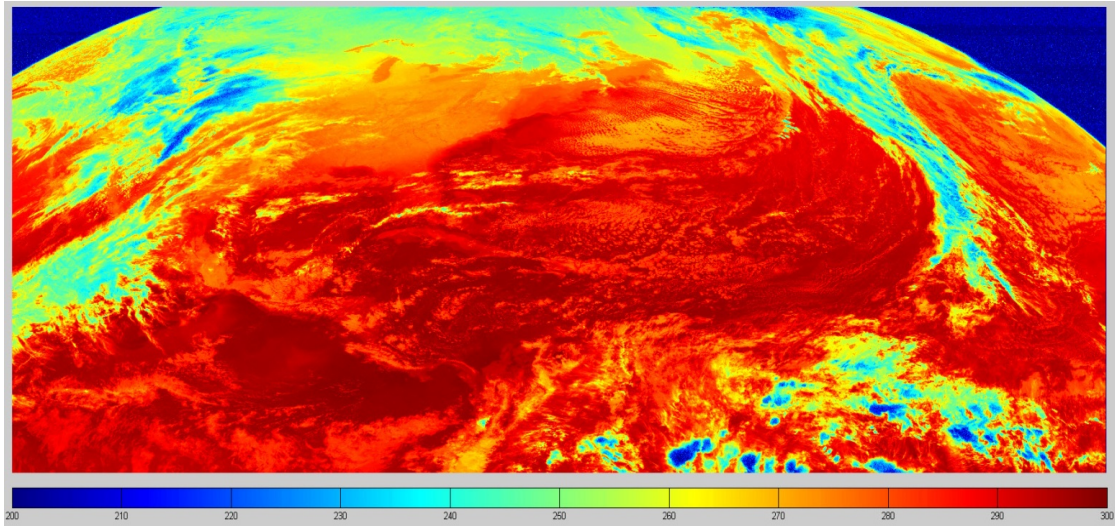
Figure 5-2 GOES measurement after calibration

5.2　Implementation of the LST algorithms

5.2.1 The new TES method

The new TES method is applied to the two GOES-8 observations acquired at 9:00 a.m. and 10:00 a.m. on July 14th, 1997. The monthly average brightness temperature measured by GOES-8 on July, 1997 is shown in Figure 5-3. The two-time measurements (9:00 a.m. and 10:00 a.m. UTM, July 14th, 1997) from Channel 4 and Channel 5 measurements of GOES-8 Imagers are shown in Figure 5-4 and Figure 5-5, respectively. Since the algorithm is sensitive to cloud conditions, it is only applied to cloud free pixels to calculate LST and emissivities. The cloud fractions (available from NOAA GOES Surface and Insolation Products) at 9 a.m. and 10 a.m. (July 14th, 1997) are shown in Figure 5-6 and Figure 5-7. Figure 5-8 and Figure 5-9 show the LST retrievals at 9 a.m. and 10 a.m., respectively. Figure 5-10 and Figure 5-11 are retrieved emissivities at 11 μm and 12 μm, respectively.

39

The spatial variation of retrieved temperatures shown in Figure 5-8 and Figure 5-9 are mostly latitudinal. The majority of the southern area is warmer than the northern counterpart. The highest temperatures appeared in the region of low latitudes, like southern Texas. Besides, extremely high temperatures are detected in the arid and hot desert in south eastern California. The emissivity of north western U.S. continent is generally higher than that of south-eastern U.S. This distribution is similar to that of the MODIS monthly emissivity product (Wan 2008).
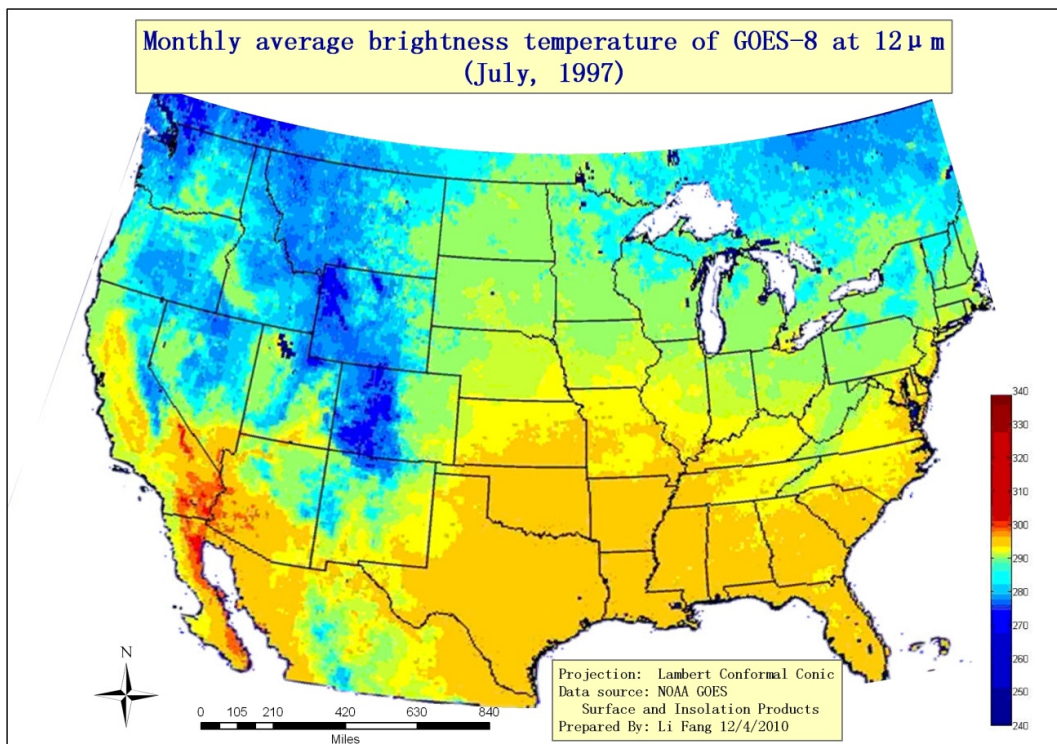
Figure 5-3 Monthly average brightness temperature of GOES-8 at $12\mu m$(July, 1997)
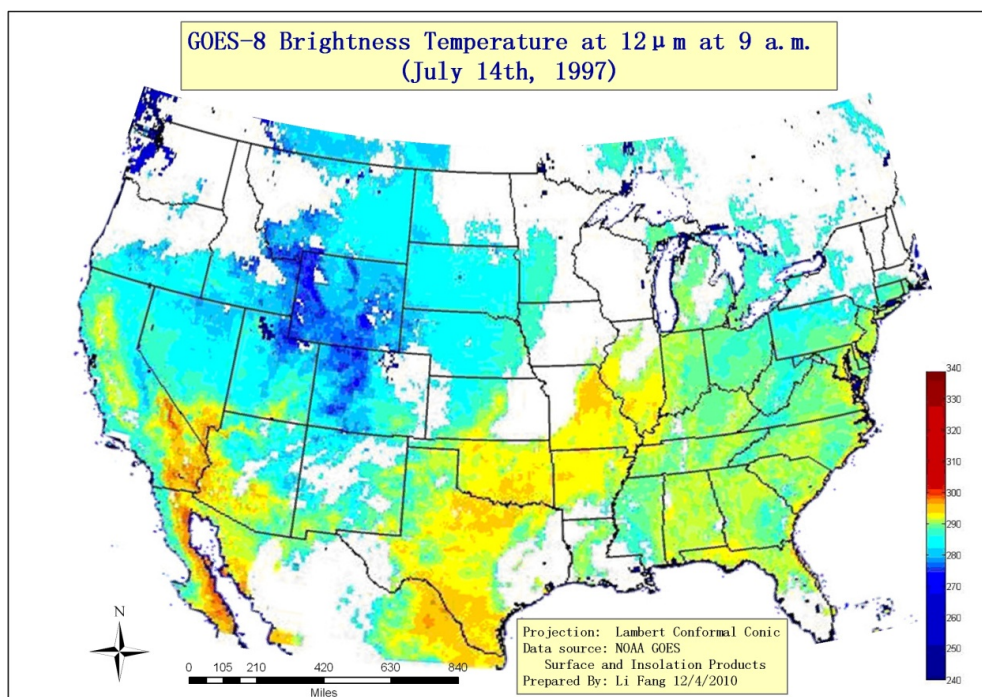
Figure 5-4 GOES-8 brightness temperature at 12µm at 9 a.m. (July 14th, 1997)
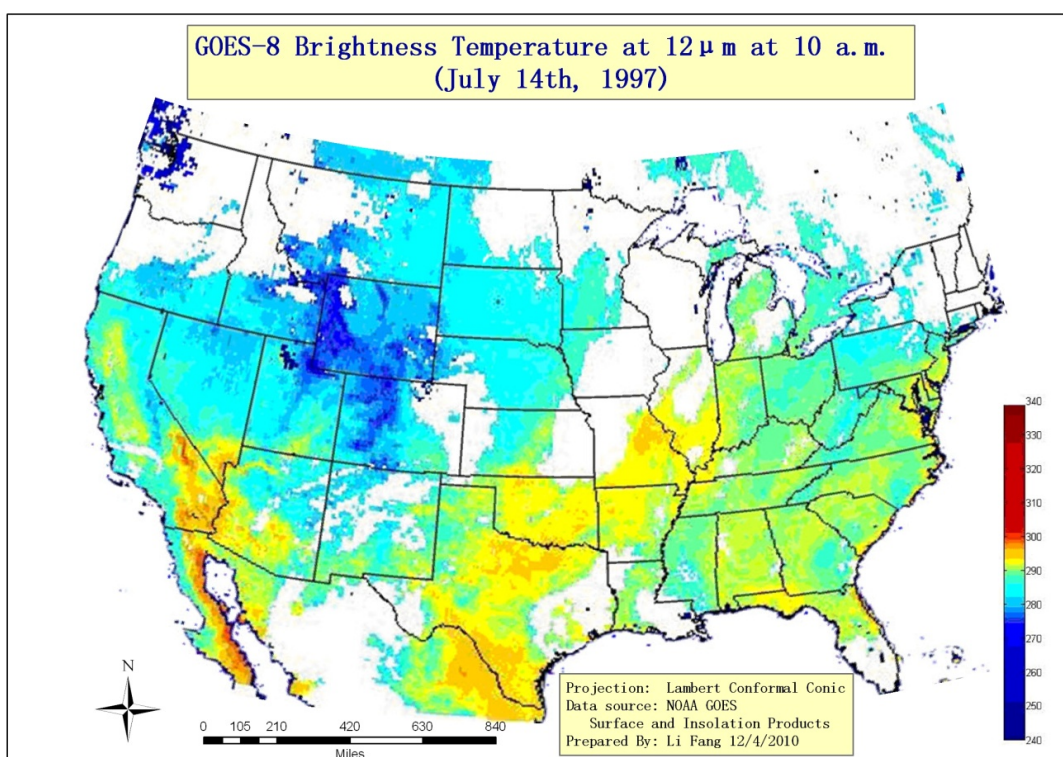
Figure 5-5 GOES-8 brightness temperature at 12µm at 10 a.m. (July 14th, 1997)
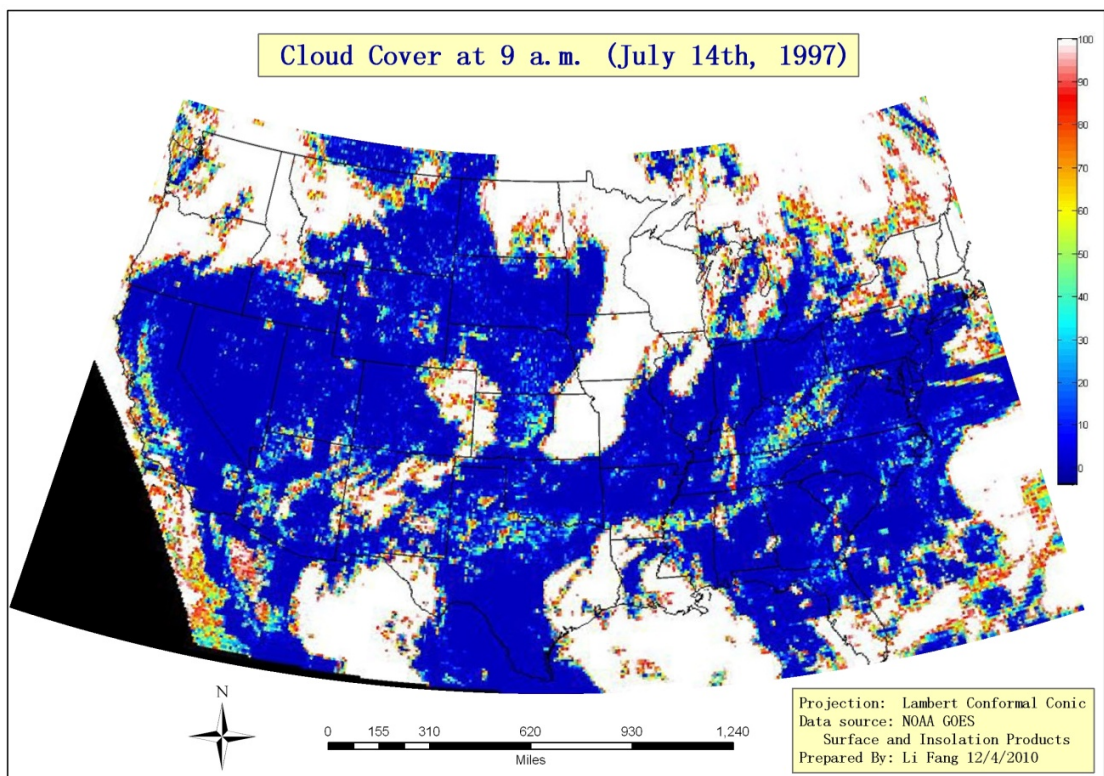
Figure 5-6 Cloud cover at 9 a.m. (July 14th, 1997)
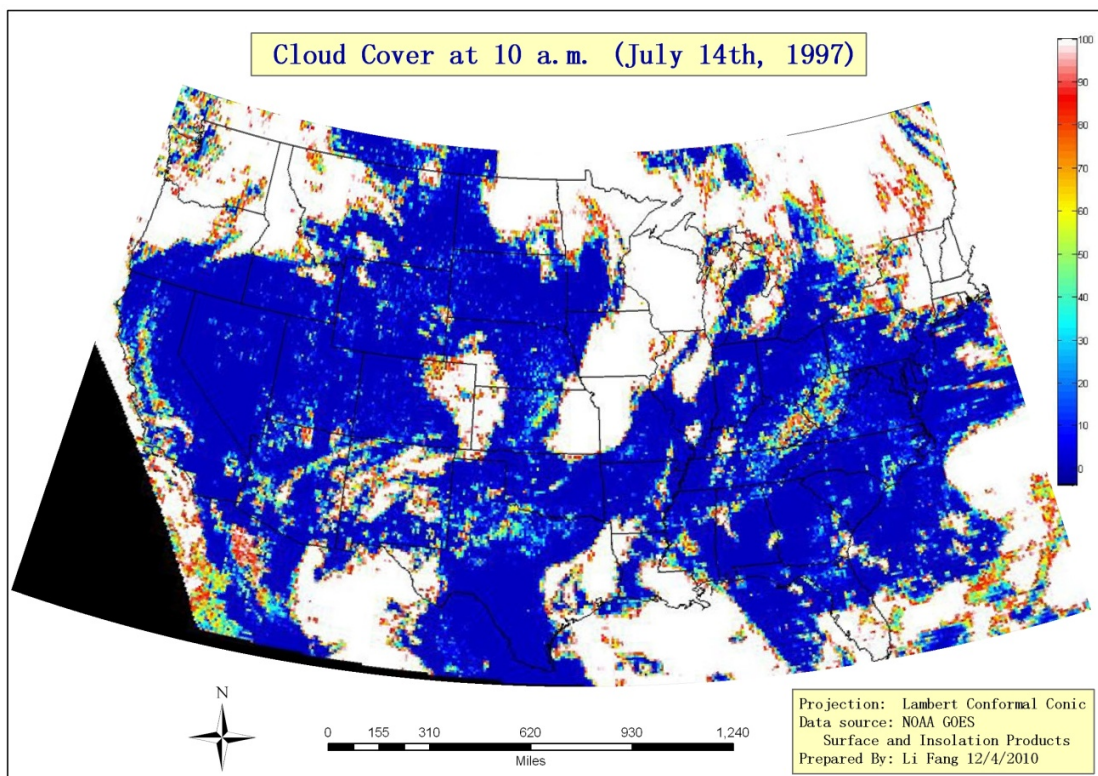
Figure 5-7 Cloud cover at 10 a.m. (July 14th, 1997)
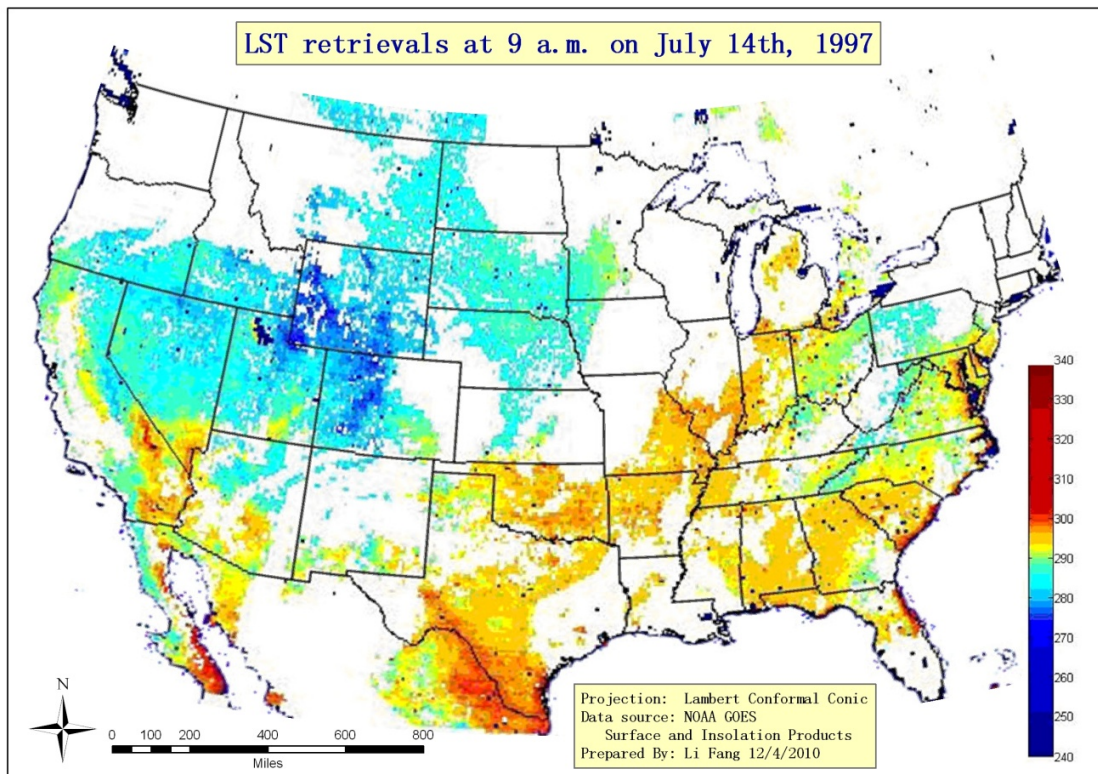
Figure 5-8 LST retrievals at 9 a.m. on July 14th, 1997.
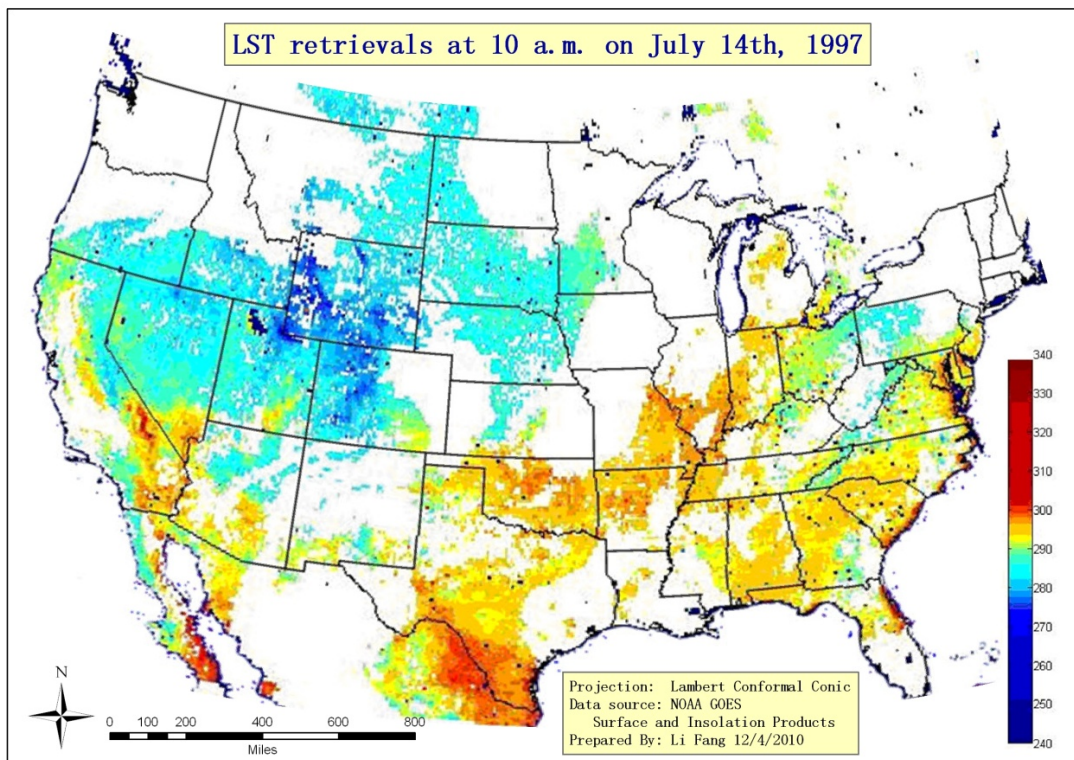
Figure 5-9 LST retrievals at 10 a.m. on July 14th, 1997.
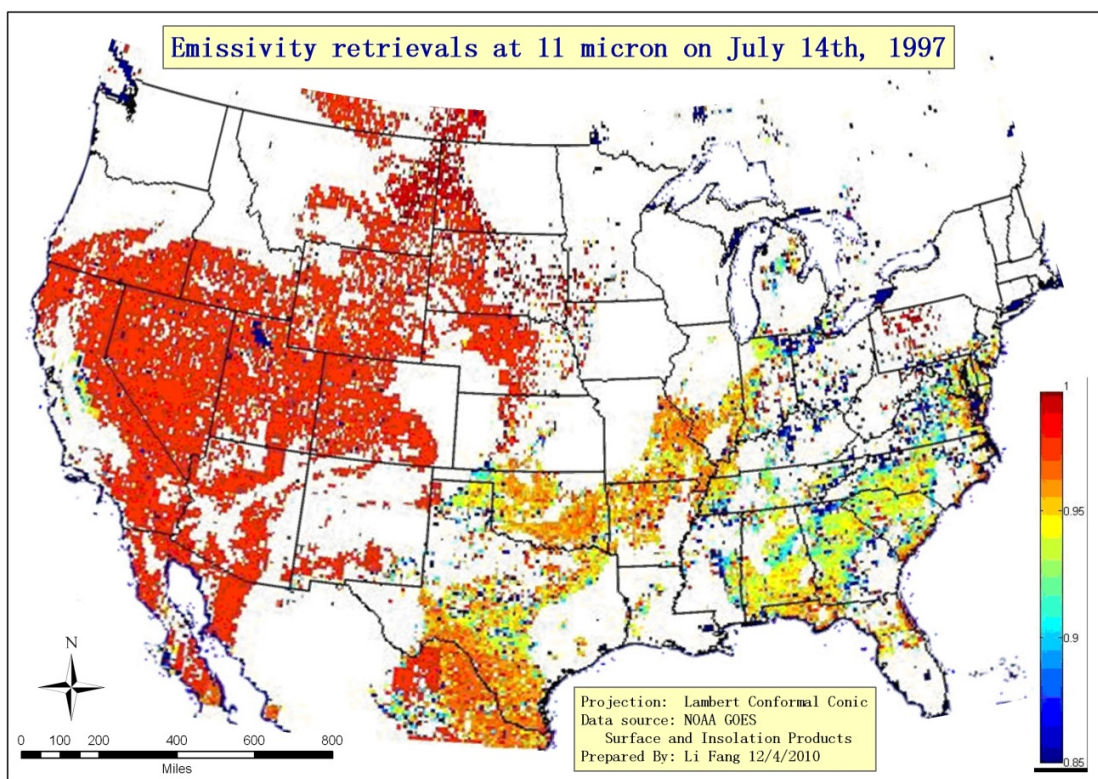
Figure 5-10 Retrieved emissivity at 11 *μm* (July 14th, 1997)
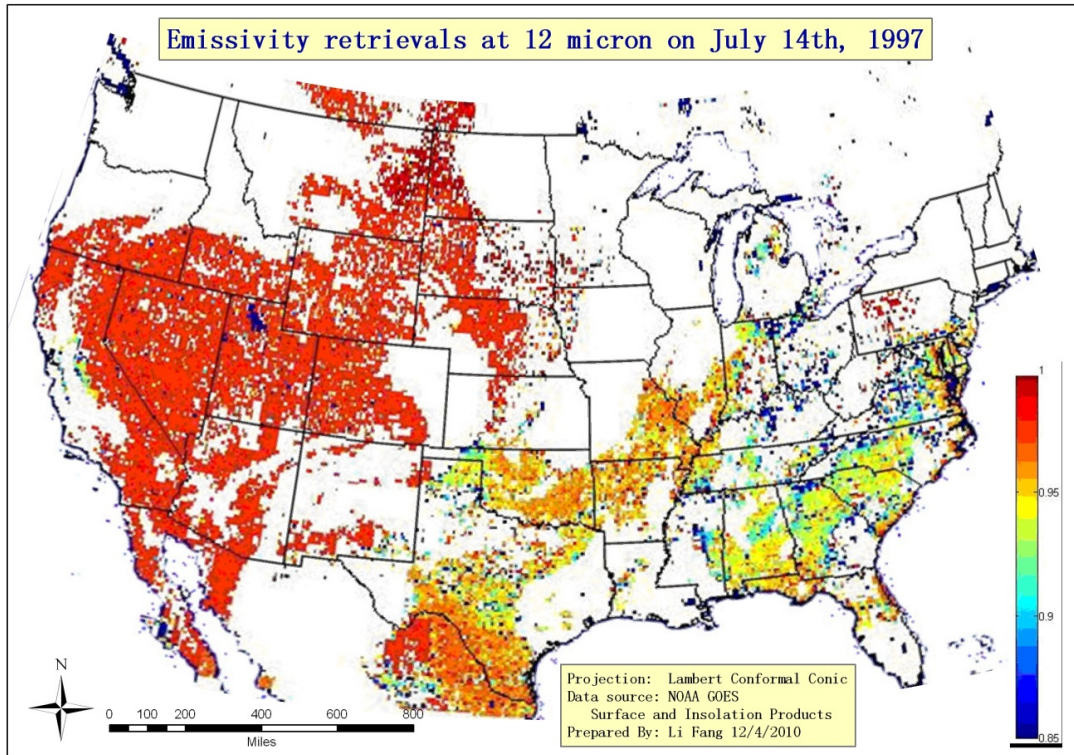
Figure 5-11 Retrieved emissivity at 12 μm (July 14th, 1997)

5.2.2 The dual-window LST algorithms with Machine learning

The dual-window LST algorithm has been applied to GOES-12 measurements from January 2004. From the whole month observations, the algorithm coefficients are obtained through the training of matched GOES brightness temperatures and SURFRAD ground-based measurements at the same time and location.

Based on the input datasets, algorithm coefficients are first generated from a conventional regression method. Algorithm coefficients for day-time and-night time are shown in Table 5-1. Statistics of LST retrieval from conventional regression method are shown in Table 5-2. From the results with traditional regression training, we can see the

results cannot meet the requirement of 2.5 K precision. The regression tree method is then applied to the same dataset. The training result is shown in Table 5-4. The training correlation coefficients for day time and night time are around 0.9 and the mean absolute errors are around 2.5K.

Table 5-1 Algorithm coefficients from conventional regression method

Time	a 0	a 1	a 2	a 3	a 4	a 5	a 6
Day time	175.9503	0.3703	-1.10670	-0.01718	24.04888	-0.00167	-41.3955
Night time	244.9676	0.1343	-0.74661	-0.11190	19.86255	0.00289	-44.1981

Table 5-2 Statistics of LST retrieval for day time

Temperature Range	Precision	Accuracy	Uncertainty	Maximum Error	Sampling No.
275.00 - 280.00	1.773	10.5544	10.7023	12.8287	6
280.00 - 285.00	2.9119	5.2842	6.0334	10.6514	39
285.00 - 290.00	3.0368	2.1595	3.7263	17.1741	303
290.00 - 295.00	4.0505	0.3796	4.0682	17.9907	468
295.00 - 300.00	4.1596	-0.0412	4.1598	14.5395	279
300.00 - 305.00	4.3836	-0.9523	4.4858	12.4006	194
305.00 - 310.00	4.2899	-2.4878	4.9591	16.8173	98
310.00 - 315.00	5.2491	-3.4572	6.2853	11.6495	46
315.00 - 320.00	4.8057	-2.7836	5.5536	11.4238	35
200.00 - 320.00	4.3663	0.2758	4.375	17.9907	1468

Table 5-3 Statistics of LST retrieval for night time

Temperature Range	Precision	Accuracy	Uncertainty	Maximum Error	Sampling No.
275.00 - 280.00	0.9887	11.8219	11.8631	13.5231	6
280.00 - 285.00	2.0253	6.3193	6.636	11.2979	38
285.00 - 290.00	1.7653	1.9859	2.6571	6.3432	281
290.00 - 295.00	1.9598	-1.2809	2.3413	7.6159	354
295.00 - 300.00	3.3289	-1.7759	3.773	8.549	151
300.00 - 305.00	2.463	-1.6577	2.9689	8.3787	46
305.00 - 310.00	2.3326	-5.48	5.9558	10.9977	13
200.00 - 320.00	3.2618	0	3.2618	13.5231	889

Table 5-4 Machine training result

(GOES-12 measurements of July 2004)

Data Source	Time	Ground-based Temperature	Sample size	Training result		
				Correlation coefficient	Mean absolute error	precision
CLASS	Day time	SURFRAD	105	0.9793	2.6264	1.2558
CLASS	Night time	SURFRAD	861	0.8895	2.5788	2.6482

```
soz <= 70.3 : LM1 (497/51.419%)

soz >  70.3 :
|   (sec(stz)-1.) <= 0.399 :
|   |    Tb11 <= 289.95 :
|   |    |    Tb11 <= 284.25 : LM2 (49/22.849%)
|   |    |    Tb11 >  284.25 : LM3 (162/26.724%)
|   |    Tb11 >  289.95 :
|   |    |    Tb11 <= 292.75 :
|   |    |    |    (sec(stz)-1.) <= 0.338 :
|   |    |    |    |    (Tb3.9-Tb11) <= 2.35 : LM4 (39/25.375%)
|   |    |    |    |    (Tb3.9-Tb11) >  2.35 : LM5 (55/19.789%)
|   |    |    |    (sec(stz)-1.) >  0.338 :
|   |    |    |    |    Tb3.9*cos(soz) <= 173.972 : LM6 (72/24.417%)
|   |    |    |    |    Tb3.9*cos(soz) >  173.972 :
|   |    |    |    |    |    (Tb3.9-Tb11) <= 1.4 : LM7 (17/27.951%)
|   |    |    |    |    |    (Tb3.9-Tb11) >  1.4 : LM8 (9/21.196%)
|   |    |    Tb11 >  292.75 : LM9 (54/19.391%)
|   (sec(stz)-1.) >  0.399 :
|   |    (sec(stz)-1.) <= 0.855 :
|   |    |    (1-ems) <= 0.032 :
|   |    |    |    Tb11 <= 289.65 :
|   |    |    |    |    Tb11 <= 285.25 : LM10 (32/13.478%)
|   |    |    |    |    Tb11 >  285.25 : LM11 (42/9.933%)
|   |    |    |    Tb11 >  289.65 :
|   |    |    |    |    soz <= 91.05 :
|   |    |    |    |    |    Tb3.9*cos(soz) <= -205.606 : LM12 (3/3.038%)
|   |    |    |    |    |    Tb3.9*cos(soz) >  -205.606 : LM13 (8/9.606%)
|   |    |    |    |    soz >  91.05 :
|   |    |    |    |    |    soz <= 113.4 :
|   |    |    |    |    |    |    Tb11 <= 291.25 : LM14 (10/4.911%)
|   |    |    |    |    |    |    Tb11 >  291.25 : LM15 (10/4.682%)
|   |    |    |    |    |    soz >  113.4 : LM16 (6/4.052%)
|   |    |    (1-ems) >  0.032 :
|   |    |    |    Tb11 <= 289.95 :
|   |    |    |    |    Tb11 <= 285.85 : LM17 (166/31.369%)
|   |    |    |    |    Tb11 >  285.85 :
|   |    |    |    |    |    (Tb3.9-Tb11)^2 <= 0.905 : LM18 (73/20.981%)
|   |    |    |    |    |    (Tb3.9-Tb11)^2 >  0.905 : LM19 (37/28.525%)
|   |    |    |    Tb11 >  289.95 : LM20 (71/33.84%)
|   |    (sec(stz)-1.) >  0.855 :
|   |    |    Tb11 <= 288.1 :
|   |    |    |    soz <= 88.25 :
|   |    |    |    |    soz <= 83.85 : LM21 (10/16.105%)
|   |    |    |    |    soz >  83.85 : LM22 (11/10.213%)
|   |    |    |    soz >  88.25 :
|   |    |    |    |    soz <= 103.25 :
|   |    |    |    |    |    (Tb3.9-Tb11) <= 2.9 : LM23 (13/16.552%)
|   |    |    |    |    |    (Tb3.9-Tb11) >  2.9 : LM24 (10/11.962%)
|   |    |    |    |    soz >  103.25 : LM25 (55/17.966%)
|   |    |    Tb11 >  288.1 : LM26 (34/12.18%)
```

The regression tree based on the sample data is shown above. The tree nodes are all variables in Eq. 3-10 "soz" stands for solar zenith angle; "stz" stands for satellite zenith angle; "Tb11" stands for T_{11}; "ems" stands for ε. All the LM models are listed below.

LM num: 1
LST =
 -0.1163 * soz
 + 31.1268 * (sec(stz)-1.)
 + 0.1409 * Tb11
 + 0.0173 * (Tb3.9-Tb11)
 - 0.0002 * (Tb3.9-Tb11)^2
 + 0 * Tb3.9*cos(soz)
 - 42.8102 * (1-ems)
 + 252.9434

LM num: 2
LST =
 -0.0476 * soz
 + 8.8863 * (sec(stz)-1.)
 + 0.0648 * Tb11
 - 0.2894 * (Tb3.9-Tb11)
 - 0.0001 * (Tb3.9-Tb11)^2
 + 0 * Tb3.9*cos(soz)
 - 1.9043 * (1-ems)
 + 275.8915

LM num: 3
LST =
 -0.0473 * soz
 + 47.484 * (sec(stz)-1.)
 + 0.2212 * Tb11
 + 0.9213 * (Tb3.9-Tb11)
 - 0.0001 * (Tb3.9-Tb11)^2
 + 0 * Tb3.9*cos(soz)
 - 1.9043 * (1-ems)
 + 213.1048

LM num: 4
LST =
 -0.0053 * soz
 + 11.672 * (sec(stz)-1.)
 + 1.154 * Tb11
 + 0.2987 * (Tb3.9-Tb11)
 + 0.0285 * (Tb3.9-Tb11)^2
 + 0 * Tb3.9*cos(soz)

- 1.9043 * (1-ems)
  - 50.1612

LM num: 5
LST =
 -0.0053 * soz
 + 11.672 * (sec(stz)-1.)
 + 0.2857 * Tb11
 + 0.2395 * (Tb3.9-Tb11)
 + 0.0285 * (Tb3.9-Tb11)^2
 + 0 * Tb3.9*cos(soz)
 - 1.9043 * (1-ems)
 + 204.75

LM num: 6
LST =
 -0.0053 * soz
 + 11.4714 * (sec(stz)-1.)
 + 0.1322 * Tb11
 + 0.2851 * (Tb3.9-Tb11)
 - 0.0893 * (Tb3.9-Tb11)^2
 + 0 * Tb3.9*cos(soz)
 - 1.9043 * (1-ems)
 + 250.9104

LM num: 7
LST =
 -0.0053 * soz
 + 11.4714 * (sec(stz)-1.)
 + 0.1322 * Tb11
 + 1.1972 * (Tb3.9-Tb11)
 - 0.2206 * (Tb3.9-Tb11)^2
 + 0 * Tb3.9*cos(soz)
 - 1.9043 * (1-ems)
 + 250.5369

LM num: 8
LST =
 -0.0053 * soz
 + 11.4714 * (sec(stz)-1.)
 + 0.1322 * Tb11
 + 0.1775 * (Tb3.9-Tb11)
 - 0.2206 * (Tb3.9-Tb11)^2
 + 0 * Tb3.9*cos(soz)
 - 1.9043 * (1-ems)
 + 250.231

LM num: 9

LST =
 -0.0792 * soz
 + 39.2267 * (sec(stz)-1.)
 + 0.1718 * Tb11
 + 0.0399 * (Tb3.9-Tb11)
 + 0.0319 * (Tb3.9-Tb11)^2
 + 0 * Tb3.9*cos(soz)
 - 1.9043 * (1-ems)
 + 238.2564

LM num: 10
LST =
 -0.0151 * soz
 + 4.8917 * (sec(stz)-1.)
 + 0.0867 * Tb11
 + 0.3539 * (Tb3.9-Tb11)
 - 0.0001 * (Tb3.9-Tb11)^2
 + 0 * Tb3.9*cos(soz)
 - 8.2748 * (1-ems)
 + 268.2738

LM num: 11
LST =
 -0.0151 * soz
 + 4.8917 * (sec(stz)-1.)
 - 0.1624 * Tb11
 + 0.2047 * (Tb3.9-Tb11)
 - 0.0001 * (Tb3.9-Tb11)^2
 + 0 * Tb3.9*cos(soz)
 - 8.2748 * (1-ems)
 + 340.6268

LM num: 12
LST =
 0.063 * soz
 + 4.8917 * (sec(stz)-1.)
 + 0.2795 * Tb11
 + 0.3807 * (Tb3.9-Tb11)
 - 0.0001 * (Tb3.9-Tb11)^2
 - 0.0028 * Tb3.9*cos(soz)
 - 8.2748 * (1-ems)
 + 208.5952

LM num: 13
LST =
 0.0519 * soz
 + 4.8917 * (sec(stz)-1.)
 + 0.2795 * Tb11

+ 0.3807 * (Tb3.9-Tb11)
- 0.0001 * (Tb3.9-Tb11)^2
- 0.0022 * Tb3.9*cos(soz)
- 8.2748 * (1-ems)
+ 209.2599

LM num: 14
LST =
 -0.0122 * soz
 + 4.8917 * (sec(stz)-1.)
 + 0.3173 * Tb11
 + 0.3105 * (Tb3.9-Tb11)
 - 0.0001 * (Tb3.9-Tb11)^2
 + 0.0004 * Tb3.9*cos(soz)
 - 8.2748 * (1-ems)
 + 202.4238

LM num: 15
LST =
 -0.0357 * soz
 + 4.8917 * (sec(stz)-1.)
 + 0.3173 * Tb11
 + 0.3105 * (Tb3.9-Tb11)
 - 0.0001 * (Tb3.9-Tb11)^2
 + 0 * Tb3.9*cos(soz)
 - 8.2748 * (1-ems)
 + 204.9661

LM num: 16
LST =
 -0.0268 * soz
 + 4.8917 * (sec(stz)-1.)
 + 0.3163 * Tb11
 + 0.3105 * (Tb3.9-Tb11)
 - 0.0001 * (Tb3.9-Tb11)^2
 + 0 * Tb3.9*cos(soz)
 - 8.2748 * (1-ems)
 + 204.1748

LM num: 17
LST =
 -0.0088 * soz
 + 14.7171 * (sec(stz)-1.)
 + 0.0507 * Tb11
 + 0.9589 * (Tb3.9-Tb11)
 - 0.0001 * (Tb3.9-Tb11)^2
 + 0 * Tb3.9*cos(soz)
 - 4.681 * (1-ems)

+ 265.8688

LM num: 18
LST =
 -0.0113 * soz
 + 3.4094 * (sec(stz)-1.)
 + 0.056 * Tb11
 + 0.228 * (Tb3.9-Tb11)
 + 0.9345 * (Tb3.9-Tb11)^2
 - 0.0014 * Tb3.9*cos(soz)
 - 4.681 * (1-ems)
 + 273.3429

LM num: 19
LST =
 -0.0131 * soz
 + 3.4094 * (sec(stz)-1.)
 + 0.056 * Tb11
 + 0.2622 * (Tb3.9-Tb11)
 + 0.0366 * (Tb3.9-Tb11)^2
 - 0.0004 * Tb3.9*cos(soz)
 - 4.681 * (1-ems)
 + 275.031

LM num: 20
LST =
 -0.0143 * soz
 + 2.5918 * (sec(stz)-1.)
 + 0.5193 * Tb11
 + 0.1772 * (Tb3.9-Tb11)
 + 0.0673 * (Tb3.9-Tb11)^2
 + 0.0026 * Tb3.9*cos(soz)
 - 4.681 * (1-ems)
 + 142.4011

LM num: 21
LST =
 0.8285 * soz
 + 2.6176 * (sec(stz)-1.)
 + 0.4466 * Tb11
 + 0.5955 * (Tb3.9-Tb11)
 + 0.3331 * (Tb3.9-Tb11)^2
 + 0.0003 * Tb3.9*cos(soz)
 - 5.265 * (1-ems)
 + 98.1796

LM num: 22
LST =

0.3668 * soz
+ 2.6176 * (sec(stz)-1.)
+ 0.2745 * Tb11
+ 0.5955 * (Tb3.9-Tb11)
+ 0.3203 * (Tb3.9-Tb11)^2
+ 0.0003 * Tb3.9*cos(soz)
- 5.265 * (1-ems)
+ 185.1115

LM num: 23
LST =
 -0.0702 * soz
+ 2.6176 * (sec(stz)-1.)
- 0.0079 * Tb11
+ 0.6601 * (Tb3.9-Tb11)
- 0.0712 * (Tb3.9-Tb11)^2
+ 0.0003 * Tb3.9*cos(soz)
- 5.265 * (1-ems)
+ 307.9789

LM num: 24
LST =
 -0.0459 * soz
+ 2.6176 * (sec(stz)-1.)
+ 0.002 * Tb11
+ 0.6481 * (Tb3.9-Tb11)
- 0.0712 * (Tb3.9-Tb11)^2
+ 0.0003 * Tb3.9*cos(soz)
- 5.265 * (1-ems)
+ 302.5407

LM num: 25
LST =
 0.0571 * soz
+ 2.6176 * (sec(stz)-1.)
+ 0.0025 * Tb11
+ 0.874 * (Tb3.9-Tb11)
+ 0.1801 * (Tb3.9-Tb11)^2
+ 0.0003 * Tb3.9*cos(soz)
- 5.265 * (1-ems)
+ 288.6851

LM num: 26
LST =
 -0.0087 * soz
+ 2.6176 * (sec(stz)-1.)
+ 0.5576 * Tb11
+ 0.7354 * (Tb3.9-Tb11)

- 0.0001 * (Tb3.9-Tb11)^2
+ 0.0007 * Tb3.9*cos(soz)
- 5.265 * (1-ems)
+ 139.0177

As we can see from the results, the precision from conventional training is 4.3K for day time samples, and 3.2K for night time. Results from regression tree give the precision of 2.6264K during day time and 2.5788K during night time.

5.3   Validation

5.3.1 GOES 8-11/R

The Near-Surface Observation Data Set-1997 (NESOB-97) from the U.S. ARM facility is utilized to validate the LST retrievals from the new TES retrieval algorithm. The continuous temperature observations with a thirty-minute interval were acquired at the ARM Cloud and Radiation Testbed (ARM/CART) site which is located at Lamont, Oklahoma (36.607ºN, 97.489ºW). Multi-Filter Radiometer is used to detect the diffuse/total upwelling irradiance, which is then converted to the skin temperature based on the NOAA/Atmospheric Turbulence and Diffusion Division algorithm (Peppler, Lamb et al. 1996; Flynn and Hodges 2005). The consistency and easy availability of the ARM data make it a favorable observation dataset to validate the retrievals from remotely sensed data. The ARM data have been adopted by Pinker et al. (Pinker, Sun et al. 2009) and Faysash and Smith (Faysash and Smith 1999) to estimate the performance of LST retrievals from the GOES satellite observations.

The LSTs retrieved from cloud-free GOES-8 thermal infrared measurements are compared with the ARM ground-based observations at the same location and at the same time. The retrieved LST and LSE, the ground-measured temperature, as well as the biases

are listed in Table 5-5. To better demonstrate the validation, the differences between ground-measured and retrieved temperatures are graphically presented in Figure 5-12. The brightness temperatures from the original data are also shown in the figure for ease of comparison. As can be seen from Table 5-5 and Figure 5-12, the satellite-retrieved temperatures agree with the ground observations very well. The skin temperature shows an overall increase by 1.24K from July 1st to July 28th with small fluctuation in between. The absolute difference between retrieved and ground-measured temperatures reaches the smallest (0.07K) on July 27th and the largest (1.15K) on July 25th. The mean absolute error and root mean squared (RMS) error of retrieved LST against the ARM measurements are 0.45K and 0.31K, respectively. The retrieved emissivity at 11μm differs very little from that at 12 μm with the mean absolute difference of merely 0.0088. The same pattern can be found in the MODIS monthly emissivity product over the U.S. continent of July 1997, in which the mean emissivity at MODIS Channel 31 (10.78 -11.28 μm) and Channel 32 (11.77 -12.27 μm) are 0.752821 and 0.754554, respectively. We also notice from the retrieved emissivity that the emissivity varies within the month at the rate of 3.4%. In summary, the new TES algorithm retrieved reasonable temperatures and emissivity with good accuracy.

Table 5-5 Ground-based observations and retrieved temperatures

Date t1:9 a.m., t2:10 a.m.	Retrieved temperature (RT) (K)	Ground-observed Temperature (GT) (K)	Differences between GT and RT	Retrieved emissivity at Channel4	Retrieved emissivity at Channel5
070/10/97 (t1)	295.82	295.48	0.34	0.96188	0.95387
070/10/97 (t2)	295.56	295.09	0.47	0.96188	0.95387
07/12/97 (t1)	296.14	296.24	0.10	0.97147	0.9684
07/12/97 (t2)	296.17	295.83	0.34	0.97147	0.9684
07/14/97 (t1)	296.62	297.18	0.56	0.93849	0.92109
07/14/97 (t2)	297.05	296.98	0.07	0.93849	0.92109
07/24/97 (t1)	297.33	297.66	0.33	0.96316	0.95656
07/24/97 (t2)	297.7	297.46	0.24	0.96316	0.95656
07/25/97 (t1)	297.86	297.16	0.70	0.95739	0.94943
07/25/97 (t2)	297.83	296.68	1.15	0.95739	0.94943
07/27/97 (t1)	296.68	297.44	0.76	0.96353	0.95398
07/27/97 (t2)	296.35	296.28	0.07	0.96353	0.95398
07/28/97 (t1)	297.57	297.94	0.37	0.95829	0.94913
07/28/97 (t2)	297.06	297.83	0.77	0.95829	0.94913
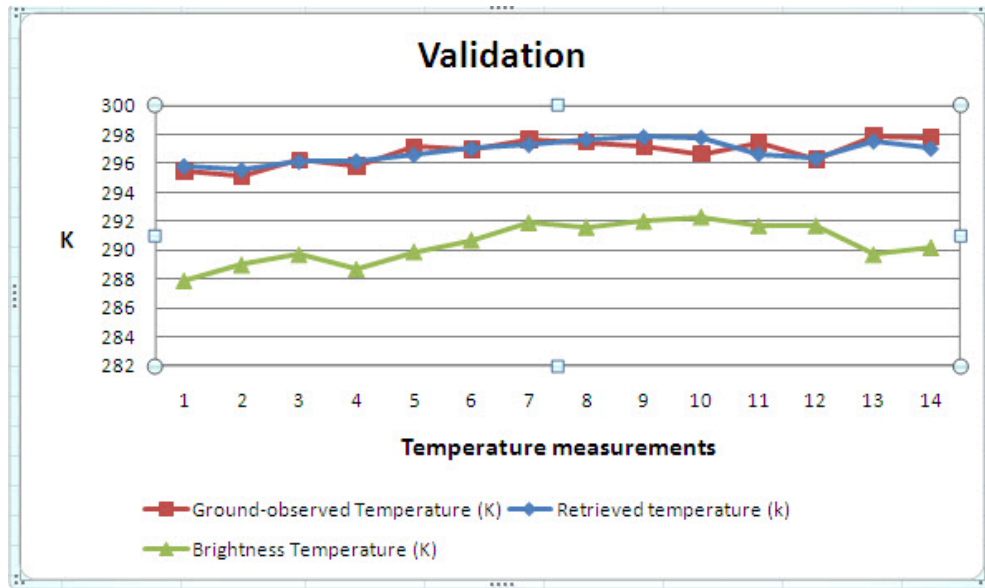
Figure 5-12 Validation results for the LST retrievals, using the dataset from U.S. Atmospheric Radiation Measurement (ARM) facility

5.3.2 GOES M-Q

Table 5-7 shows the evaluation results of the GOES-12 LST retrievals against the SURFRAD observations at the six stations. The station ID (TSAID) of SURFRAD six observation sites are listed in Table 5-6. The accuracy (ACC), precision (Prec) and N represent the mean bias (difference), and standard deviation error between GOES LSTs and SURFRAD observations. N indicates the total sample numbers.

Table 5-6 List of SURFRAD observation sites

Site No.	Site Location	Lat(N)/Lon(W)	Surface Type*
1	Bondville, IL	40.05/88.37	Crop Land
2	Fort Peck, MT	48.31/105.10	Grass Land
3	Goodwin Creek, MS	34.25/89.87	Deciduous Forest
4	Table Mountain, CO	40.13/105.24	Crop Land
5	Desert Rock, NV	36.63/116.02	Open Shrub Land
6	Pennsylvania State University, PA	40.72/77.93	Mixed Forest

*IGBP surface types

Table 5-7 Accuracy/Precision Estimations of Four Mid-seasons months from GOES-12 LST Retrieval

Site No.	January			April			July			October		
	N	Acc	Prec	N	Acc	Prec	N	Acc	Prec	N	Acc	Prec
1	164	-1.64	1.46	120	-1.83	1.93	151	-2.18	1.49	121	-0.32	1.75
2	188	-1.27	2.28	71	-2.88	1.54	146	-2.94	1.48	74	-0.38	2.57
3	208	-1.13	1.64	183	-1.53	1.89	104	-2.89	1.43	163	0.12	1.81
4	206	-0.53	2.15	145	-0.02	2.28	209	0.11	1.95	192	-1.01	1.85
5	182	-1.33	2.00	127	-1.42	2.49	167	-1.41	2.08	135	-0.13	2.65
6	133	-1.68	2.34	99	-1.46	2.23	169	-1.08	2.30	133	1.56	2.65

Shown in Table 5-7 are the accuracy/precision values for the four seasons, respectively. It is worth of noting that the seasonal precision values are still around 2.5K. But the seasonal accuracy patterns vary from site to site. It is unsure whether such distinct

seasonal patterns might be related to the different surface covers and regional climates. All these statistical features will be further studied in the future.

Big errors are found in winter, especially over cold surfaces where surface temperatures are below the freezing point or less than 273 K or 0º C. A possible reason for this may be the snow contamination. Therefore, snow and snow-free cases are analyzed separately, as shown in Table 5-8. However, it is found that snow-free cases don't show improvements to the precision. As shown in Table 5-9, for the pixels with snow cover less than 5%, there are still many pixels with extremely low observed brightness temperature, which can be different from the SURFRAD measurements as big as 28 degrees. Big retrieval errors are caused by these pixels with extremely low temperature.

In the next step, temperatures of cloud and snow cover pixels are analyzed. For cloudy pixels, as shown in Table 5-10, the average temperatures of GOES measurement at 11µm and ground observations for all the pixels with cloud cover possibility larger than 90% are computed, which are 252.27 and 270.55, respectively. The average difference can reach as large as 18 degrees. While for snow pixels with snow cover larger than 5% (Table 5-11), average brightness temperature at 11 µm is not that different from the ground measurements. The mean difference is less than 5 degrees. From this analysis, a safe conclusion can be drawn that the big differences are more probably not caused by snow, but rather by cloud contamination, which the cloud cover algorithm may fail to detect. If all these contaminative pixels with the T_{11} less than the average cloud top temperature, then the results show many improvements (Table 5-12).

Table 5-8 Accuracy/Precision estimations from LST retrieval from GOES-12 for Jan. 2004

Date	Time	Ground Temperature	Sample size	Correlation coefficient	Bias error	Precision
0401	daytime	SURFRAD	98	0.9554	1.6401	2.3280
0401	Nighttime	SURFRAD	798	0.8614	2.8162	3.0006
0401	Daytime-snowfree	SURFRAD	70	0.9448	1.7335	2.2032
0401	Nighttime-snowfree	SURFRAD	696	0.8614	2.5822	3.0233
0401	Daytime-snow	SURFRAD	13	0.9534	1.4844	0.8024
0401	Nighttime-snow	SURFRAD	32	0.9356	1.4157	0.8750

Table 5-9 Records with big errors from NCDC data (Cloud free && snow free)

T_{11}	Retrieved temperature (LST)	SURFRAD (Ts)	Differences (Ts-T_{11})	Differences (Ts-LST)	Snow cover	Cloud cover
244.983	252.481	273.544	**28.561**	21.063	0	0
259.486	262.779	284.125	**24.639**	21.347	0	0
253.324	257.159	274.78	**21.457**	17.621	0	0
253.211	258.288	273.93	**20.719**	15.642	0	0
250.29	255.969	270.233	**19.942**	14.264	0	0
255.457	259.804	275.249	**19.791**	15.445	0	0
261.585	263.889	281.067	**19.482**	17.178	0	0
266.798	269.673	285.263	**18.465**	15.59	0	0
261.753	265.402	280.157	**18.404**	14.755	0	0
251.984	258.238	269.789	**17.806**	11.551	0	0
246.885	252.16	264.61	**17.725**	12.45	0	0
259.854	264.458	277.126	**17.272**	12.669	0	0
257.4	269.883	274.586	**17.185**	4.702	0	0
263.07	265.67	280.136	**17.067**	14.466	0	0
267.701	269.405	284.76	**17.06**	15.355	0	0
267.566	288.035	284.273	**16.707**	3.762	0	0

Table 5-10 Statistics of cloud cover pixels

cloud	GOES T_{11} (K)	SURFRAD (K)	Differences (K)
Max	285.759	296.6778	68.9041
Min	214.591	236.1	0.0062
average	252.2728	270.5534	**18.40956**

Table 5-11 Statistics of snow cover pixels

snow	GOES T_{11} (K)	SURFRAD (K)	Differences (K)
Max	265.235	268.9851	27.4411
Min	223.919	247.2088	0.0141
average	254.2187	258.9029	**4.919885**

Table 5-12   Accuracy/Precision estimations from LST retrieval from GOES-12 for Jan. 2004 (cloud contaminative pixels exclusive)

Date	Time	Ground Temperature	Sample size	Correlation coefficient	Bias error	Precision
0401	daytime	Surfrad	96	0.9829	1.1725	1.3324
0401	Nighttime	Surfrad	752	0.9408	1.9687	1.8893
0401	Daytime-snowfree	Surfrad	68	0.9797	1.0963	1.3307
0401	Nighttime-snowfree	Surfrad	654	0.9422	1.8102	1.8706
0401	Daytime-snow	Surfrad	13	0.9534	1.4844	0.8024
0401	Nighttime-snow	Surfrad	32	0.9356	1.4157	0.8750

5.3.3 Error Budget

The test results shown in the above Section indicate that overall both the accuracy and precision of the selected algorithm meet requirements (2.5K). Such assessment is based on both the simulation dataset, and ground observations from the SURFRAD.

As mentioned earlier, there are several issues that should be further studied in the match-up dataset comparisons. Particularly, difference between the satellite pixel-size measurement and the ground spot-size measurement must be characterized for a high quality validation procedure.

Accuracy of the SURFRAD LST estimation is also a concern since it is calculated from the upwelling and downwelling irradiance with a broadband surface emissivity value. The emissivity values are estimated from the surface type classification and the emissivity library (Snyder, Wan et al. 1998), and MODIS narrow band emissivity, which may introduce errors to the ground LST estimation.

Cloud contamination is still a problem even if we have used a stringent cloud filtering procedure in generating the match-up dataset. It is found that a little threshold value or procedure change will have a significant impact on the output match-up data pairs, though the overall validation results are not obviously affected.

All the above factors may potentially degrade the algorithm performance.

Chapter 6 Discussion

6.1   Issues in the new TES method

Some issues relevant to the new TES algorithm need further discussion. Singularity

is a serious concern for the new algorithm. Eq.3-5 is theoretically solvable even when the

two time measurements are slightly different. However, when the two measurements are

too close in value, the solution would be inevitably significantly affected by the random

noise in the data. Cautions, therefore, must be taken to avoid singularity of Eq.3-5.   First,

the brightness temperatures (T_{11}, T_{12}) must be significantly different from different

observation times to guarantee a reliable retrieval. Usually, a sufficient time interval

between the observations can result in significant temperature difference. However, a large

time interval may break the emissivity constancy. Other authors experienced the similar

problem. Watson pointed out that the two-measurement method required distinct

temperature and emissivity invariance, which is not easy to be satisfied at the same time,

particularly for polar-orbiting satellite data (Watson 1992b). In our experiment the most

stable results were obtained when the temporal interval between the two measurements is

set in a range from one to three hours, which ensures sufficient temperature difference and

emissivity constancy at the same time. Similar temporal interval is reported by Li et al. (Li

and Schmit Sept. 2008) and Yu et al.(Yu, Xu et al. 2009). Second, the applied SW LST

algorithms, F() and G(), should be independent. It is not sufficient to identify whether the

two SW LST algorithms are independent from their formula. Experimental testing using actual satellite data is important as well. In this study, we use two sets of the SWLST algorithms developed by Yu et al. (Yu, Tarpley et al. 2009a) , which is part of their LST algorithm development for the U.S. GOES-R satellite mission. The experimental results have demonstrated the feasibility of the new TES method in practice.

The main error related to this new TES algorithm may come from (1) the accuracy limitation of the SW LST algorithms themselves; (2) sensitivity to emissivity; and (3) cloud contamination.

It is worth mentioning that the time interval does not have to be fixed to a certain value (e.g. three hours) all the time. When the measurements at three-hour interval are not available for some reason such as cloudiness, the algorithm could automatically search for observations at other time stamps within the allowed time interval (one to three hours). Considering that geostationary satellites usually can provide high temporal observations (e.g., 15 min refresh rate of GOES Imager), more data pairs would be available for the new TES retrieval process. This flexible selection method will increase the number of qualified pairs of observations, which is of great value to operational production of LST product.

6.2 Issues in the uncertainty of emissivity

We found that the solution for emissivity is not as stable as that for temperature, which may result in falsely retrieved emissivity, either negative or greater than one. The sensitivity to emissivity is understandable, which inherits the problem from which most SW LST algorithms suffer. Yu et al. (Yu, Tarpley et al. 2009a) analyzed the emissivity sensitivities of nine SW LST algorithms and indicated that small uncertainty in emissivity

could cause significant uncertainty in LST retrievals (over 3K). One option to minimize the effect brought by uncertainty in emissivity is to find the optimal combination from those SW LST algorithms that are less sensitive to emissivity. According to the previous research (Yu, Tarpley et al. 2009a), SW algorithms developed by Prata et al. and Uliveri et al. showed low sensitivity to emissivity since the emissivity differences are not introduced in the algorithms.

6.3   Issues in the angular anisotropy

The effect of angular anisotropy is not taken into account for most existing LST retrieval algorithms. Table 6-1 presents the research on the angular effects of thermal emitted radiation. It has been noticed that brightness temperature varies with sun-view geometry and the difference in brightness temperature between vertical and oblique measurements could reach as high as 9.3K for certain land types according to Paw U's research (Paw U 1992). On average, the brightness temperature varies 1-4K with the viewing angle. Meanwhile, some scientists analyzed the directional emissivity effect, which showed that the apparent emissivity varies from 0.9560 to 0.9680 (Sobrino, Li et al. 1994).

The angular anisotropy should be a concern to the future GOES LST product because of the distinct characteristics of the GOES series. Currently, the GOES series have two operational positions, GOES-W located at the west longitude of 135°W over the Pacific Ocean, and GOES-E at 75°W over the Amazon River, as shown in Figure 6-1. Measurements of the common area from GOES-E and GOES-W may be significantly

different due to the obvious different observing angles. The consistence of LST retrievals

between GOES-W and GOES-E will be a very important research topic in the future study.

Table 6-1 Some experiments and results about BRDF effects of LST/emissivity

| Date	Scientist	Land type	Research conclusion	Reference
1983	Kimes etc.	Crop canopies	Difference of BT reaches 4K between vertical and oblique measurements	(Kimes and Kirchner 1983)
1982	Doizer etc.	snow	Difference of BT reaches 3K because of directional emissivity effect	(Dozier and Warren 1982)
1987	Balick, Hutchinson	broad-leaved forest	Difference of BT reaches 7K	(Balick, Hutchison et al. 1987)
1986	Barton,Talashima	bare soil	emissivity rapidly decreases when viewing angle larger than 60°	(Barton and Talashima 1986)
1991	Labed and Stoll	bare soil	emissivity rapidly decreases when viewing angle larger than 60°	(Labed and Stoll 1991)
1992	Paw U	sunflower	The biggest difference reaches 9.3 K	(Paw U 1992)
2000	Lagouarde	corn	Difference of BT reaches 4K between vertical and oblique measurements	(Lagouarde, Ballans et al. 2000)
2000	Lagouarde	Bare soil	Difference of BT reaches 3.5K between vertical and oblique measurements	(Lagouarde, Ballans et al. 2000)
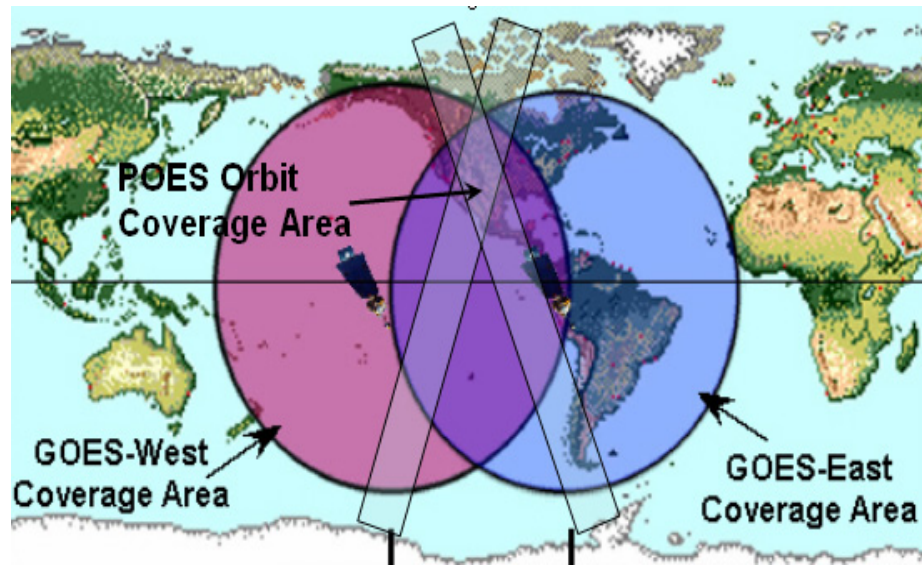
Figure 6-1 Coverage of GOES-East and GOES-West

Chapter 7 Conclusion and future work

Land surface temperature is of fundamental importance to the net radiation budget at the Earth's surface and it is also an important indicator for both the greenhouse effect and the energy exchange between the atmosphere and earth surface. Compared to the sparely distributed in-situ surface air temperature measurements, the use of satellite-derived data could contribute to a large-area consistent measurement (Gallo, Owen et al. 1999). Satellite LSTs, when assimilated into climate, mesoscale atmospheric and land surface models, are capable of analyzing long term climate change on large scales due to their rich archive which is routinely produced from satellite imagery data. Since surface temperature has a strong diurnal cycle, and since only geostationary satellites are capable of providing good diurnal coverage, the consistent LSTs from GOES series will substantially improve the accuracy of global and mesoscale modes, and allow the estimation of DTR, which is an important climate change indicator.

According to the unique characteristics of the GOES series, two sets of LST retrieval algorithms are presented in this study to generate consistent land surface temperatures from GOES-8 to GOES-14.

The new TES method is described in detail to derive temperature and emissivity simultaneously from two-time TIR observations from GOES 8 to GOES 11 as well as the new generation (GOES R). This method has the advantage of simplicity in using two

measurements within a period of time without having to solve radiative transfer equations. The flexibility of integration of the established LST retrieval algorithms makes the method easy to implement. Two combinations of SW LST algorithms are adapted in this method, and both produce reasonable results. Validation results demonstrate that the TES algorithm is capable of simultaneously deriving qualified LST and LSE with good retrieval precision. The bias error of the algorithm is estimated around 1.15K.

A machine learning technique using a regression tree method has been introduced to the dual-window LST algorithm to retrieve LSTs from GOES M (12) to GOES Q. The advantages of the regression tree method make it attractive for applications that operationally derive LSTs with high accuracy. RT can provide flexible and robust analytical methods for identifying the relationships between complex environmental data (De'ath and Fabricius 2000). The application of RT techniques to LST retrieval is innovative and creative, with real potential to make contributions about how to determine regression relationships under different conditions. That is certainly an evolutionary step in the use of massive, dynamic, ambiguous and possibly conflicting digital data. The evaluation results between GOES 12 and SURFRAD observations shows that the seasonal retrieval precision is around 2.5K, around 1K improvement compared to the conventional training method.

Error sources have been carefully analyzed for the new TES algorithm as well as the dual-window LST algorithm. The main error related to the TES retrieval algorithm may come from (1) the accuracy limitation of the SW LST algorithms themselves; (2) sensitivity to emissivity; and (3) cloud contamination.

For the new TES method, further study is necessary for the completeness and practicality of this algorithm. First, only two combinations of SW LST algorithms have been selected and implemented here. Combinations of other existing SW LST algorithms are also feasible in theory and effective in practice, but their retrieval precision and stability need to be investigated. Second, singularity is still a major concern for the new algorithm. More experiments in the future are needed to gain an in-depth understanding of how to choose optimal data pairs with both independent temperatures and constant emissivity.

In addition, the difficulties with comparison of satellite retrievals with ground observations are well known and common to many other satellite products. One problem of this kind is caused by the incompatibility between pixel-sized satellite observations and surface point measurements.

Finally, the large diurnal variability of LST is something that is conceptually understood, but which is poorly described quantitatively and not explicitly accounted for in the algorithm. Surface type, especially the green coverage and soil moisture, is a crucial factor for the amplitude of the diurnal cycle. Bare dry soil has a high Bowen ratio while transpiring vegetation is low, and therefore, pixels with low vegetation present much larger diurnal variation (Sun, Pinker et al. 2006). A second contributor to LST variation is the fraction of surface shadowing which can be seen from the observing satellite for the reason that shaded surfaces are significantly cooler than sunlit surfaces. And the apparent shadow fraction varies according to the relative geometry of the sun and satellite and is changing throughout daylight hours. All of these factors should be factored into the LST algorithm in future research.

References

References

Balick, L. K., B. A. Hutchison, et al. (1987). "Directional thermal Infrared Exitance Distributions of a Deciduous Forest in Summer." <u>IEEE Transactions on Geoscience and Remote Sensing</u> **25**: 410-412.

Barducci, A. and I. Pippi (1996). "Temperature and emissivity retrieval from remotely sensed imagesusing the "Grey body emissivity" method." <u>iEEE Transactions on Geoscience and Remote Sensing Letters</u> **34**(3): 681-695.

Barker, F. and Z. L. Li (1990a). "Toward a local split window method over land surface." <u>International Journal of Remote Sensing</u> **3**: 369-393.

Barker, F. and Z. L. Li (1990b). "Temperature-Independent Spectral Indices in thermal infrared bands." <u>Remote Sensing of Environment</u> **32**: 17-33.

Barton, I. J. and T. Talashima (1986). "An AVHRR investigation of surface emissivity near lake Eyre." <u>Remote Sensing of Environment</u> **1986**(20).

Becker, F. and Z. L. Li (1995). "Surface temperature and emissivity at various scales: definition, measurement and related problems." <u>Remote sensing of reveiews</u> **12**: 225-253.

Braganza, K., D. J. Karoly, et al. (2004). "Diurnal temperature ranges as an index of global climate change during the twentieth century." <u>Geophysical Research Letters</u> **31**: L13217.

Camillo, P. J. (1991). <u>Using one- or two-layer models for evaporation estimation with renotely sensed data</u>" in Land Surface Evaporation: Measuremnts and Parameterization. New York, Springer.

Caselles, V., C. Coll, et al. (1997). "Land surface temperature determinatin in the whole Hapex Sahell area from AVHRR data." International Journal of Remote Sensing **18**(5): 1009-1027.

Coll, C., C. Caselles, et al. (1994). "On the atmospheric dependence of the split-window equation for land surface temperature." International Journal of Remote Sensing **15**(1): 1915-1932.

Coll, C. and V. Caselles (1997). "A split-window algorithm for land surfaces temperature from Advanced Very High-Resolution Radiometer data: Validation and algorithm comparison." Journal of Geophysical Research **02**: 16,697-616,713.

Cresswell, M. P., A. P. Morse, et al. (1999). "Estimating surface air temperatures, from Meteosat land surface temperatures, using an empirical solar zenith angle model." International Journal of Remote Sensing **20**(6): 1125-1132.

Dash, P., F. M. Gottsche, et al. (2002). "Potential of MSG for surface temperature and emissivity estimation: considerations for real-time applications." International Journal of Remote Sensing **23**(20): 4511-4518.

De'ath, G. and K. E. Fabricius (2000). "Classification and regression trees:a powerful yet simple technique for ecological data analysis."

Dittberner, G., R. Grid, et al. (1996). "NOAA's future earth observations from advanced GOES satellites." Acta Astronautica **39**(4-8): 467-477.

Dozier, J. and S. G. Warren (1982). "Effect of viewing angle on Infrared Brightness Temperature of Snow." Water Resources Research **18**: 1424-1434.

Faysash, D. A. and E. A. Smith (1999). "Simultaneous land surface temperature–emissivity retrieved in the infrared split window." Journal of Atmospheric and Oceanic Technology **16**: 1673–1689.

Flynn, D. and G. Hodges (2005). "Multi-Filter Radiometer (MFR) Handbook." U.S. Department of Energy, Office of Science, Office of Biological and Environmental Research.

Francois, C. and C. Ottle (1996). "Atmospheric corrections in the Thermal Infrared: Global and Water Vapor Dependent Split-Window Algorithms-Applications to ATSR and AVHRR data." IEEE Transactions on Geoscience and Remote Sensing **34**(2): 457-470.

Gallo, K. P., T. W. Owen, et al. (1999). "Temperature trends of the U.S. historical climatology network based on satellite-designated land use/land cover." Journal of Climate **12**(5): 1344-1348.

Gillespie, A. R. (1985). "Lithologic mapping of Silicate Rocks using TIMS. The TIMS data User's Workshop." JPL Publication 86-38: 29-44.

Gillespie, A. R., T. Matsunaga, et al. (1998). "Temperature and emissivity separation from Advanced Spaceborne Thermal Emission and Reflection Radiometer Images." IEEE Transactions on Geoscience and Remote Sensing **36**: 1113-1126.

Gottsche, F. M. and F. S. Olesen (2001). "Modeling of diurnal cycles of brightness temperature extracted from METEOSAT data." Remote Sensing of Environment **76**(3): 337-348.

Hay, S. I. and J. J. Lennon (1999). "Deriving meteorological variables across Africa for the study and control of vector-borne disease: a comparison of remote sensing and spatial interpolation of climate." Tropical Medicine and International Health **4**(1): 58-71.

Hayden, C. M. (1988). "GOES-VAS simultaneous temperature-moisture retrieval algorithm." Journal of Applied Meteorology and Climatology **27**(6): 705-733.

Hayden, C. M., G. S. Wade, et al. (1996). "Derived product imagery from GOES-8." Journal of Applied Meteorology and Climatology **35**(2): 153-162.

Kahle, A. B. and L. C. Rowan (1980). "Evaluation of multispectral middle infrared aircraft images from lithologic mapping in the east Tintic Mountains,Utah." Geology **8**(234-239).

Karl, T. R., P. D. Jones, et al. (1993). "A New Perspective on Recent Global Warming: Asymmetric Trends of Daily Maximum and Minimum Temperature." Bulletin of the American Meteorological Society **74**: 1007-1023.

Karl, T. R., G. Kukla, et al. (1984). "Decreasing diurnal temperature range in the US climatic record." Journal of Climate Applications **23**: 1489-1504.

Kealy, P. S. and A. R. Gabell (1990). Estimation of emissivity and temperature using Alpha Coefficients. In Proc. 2nd TIMS Workshop, Pasadina, CA, JPL publication 90-55.

Kealy, P. S. and S. J. Hook (1993). "Separating temperature and emissivity in thermal infrared multispectral scanner data: Implications for recovering land surface temperature." IEEE Transactions on Geoscience and Remote Sensing **31**: 1155-1164.

Kerr, Y. H., J. P. Lagouardeb, et al. (1992). "Accurate land surface temperature retrieval from AVHRR data with use of an improved split window algorithm." Remote Sensing of Environment **41**(2-3): 197-209.

Kimes, D. S. and J. A. Kirchner (1983). "Directional radiometric measurements of row-crop temperatures." international Journal of Remote Sensing **4**: 299-311.

Kin'uyu, S. M., L. A. Ogallo, et al. (1999). "Recent Trends of Minimum and Maximum Surface Temperatures over Eastern Africa." Journal of Climate **13**: 2876-2886.

Kustas, W. P. and D. Goodrich (1994). "Preface to special section on MONSOON'90." Water Resources Research **30**: 1211-1225.

Labed, J. and M. P. Stoll (1991). "Angular variation of land surface spectral emissivity in the thermal infrared: laboratory investigations on bare soils." international Journal of Remote Sensing **12**: 2299-2310.

Lagouarde, J.-P., H. Ballans, et al. (2000). "Experimental Study of Brightness Surface Temperature Angular Variations of Maritime Pine Stands." Remote Sensing of Environment **72**: 17-34.

Li, J. and T. Schmit (Sept. 2008). "GOES-R advanced baseline imager (ABI) algorithm theoretical basis document for surface emissivity." version 1.0.

Li, Z. L. and F. Barker (1993). "Feasibility of land surface temperature and emissivity determination from AVHRR data." Remote Sensing of Environment **43**: 67-85.

Li, Z. L., F. Becker, et al. (1999). "Evaluation of six methods for extracting relative emissivity spectral from thermal infrared images." Remote Sensing of Environment **69**(3): 197-214.

Liang, S. (2001). "An optimized algorithm for separating land surface temperature and emissivity from multispectral thermal infrared imagery." IEEE Transactions on Geoscience and Remote Sensing **39**(2): 264-274.

Lorenz, D. (1986). "The effect of the long-wave reflectivity of natural surfaces on surface temperature measurements using radiometers." Journal of Applied Meteorology and Climatology **5**: 421-430.

Ma, X. L., T. J. Schmit, et al. (1999). "A non-linear physical retrieval algorithm- its application to the GOES-8/9 sounder." Journal of Applied Meteorology and Climatology **38**: 501-513.

Ma, X. L., Z. Wan, et al. (2002). "Simultaneous retrieval of atmospheric profiles, land surface temperature, and surface emissivity from Moderate Resolution Imaging Spectroradiometer thermal infrared data: extension of a two-step physical algorithm." Applied Optics **41**(5): 909-924.

Matsunaga, T. (1994). "A temperature-emissivity separation method using an empirical relationship between the mean, the maximum, and the minimum of the thermal infrared emissivity spectrum." Journal of Remote Sensing Society of Japan **14**(2): 230-241.

McMillin, L. M. (1975). "Estimation of sea surface temperature from two infrared window measurement with differenct absorption." Journal of Geophysical Research **80**: 5113-5117.

Minnett, P. J. (1986). "On the use of synthetic 12m data in a split-window retrieval of sea-surface temperature from AVHRR measurements." International Journal of Remote Sensing **7**(1887-1891).

Morcrette, J. J. (1991). "Evaluation of model-generated cloudiness-satellite observed and model-generated diurnal variability of brightness temperature." Monthly Weather Review **119**(5): 1205-1224.

Nerry, F., J. Labed, et al. (1990). "Spectral properties of land surfaces in the thermal infrared band. Part I: Laboratory measurements of absolute spectral emissivity and reflectivity signatures." Journal of Geophysical Research **95**: 7027-7044.

NOAA/NESDIS (1998). Earth location user's guide (ELUG) Revision 1**:** (available at: http://goes.gsfc.nasa.gov/text/ELUG0398.pdf).

Noyes, E., G. Corlett, et al. (2007). Future development of the operational AATSR LST product. The Second Envisat Symposium, Montreux, Switzerland.

OLesen, F. S., O. Kind, et al. (1995). "High-resolution time-series of IR data from a combination of AVHRR and METEOSAT." Advances in Space Research **16**(10): 141-146.

Ottlé, C. and D. Vidal-Madjar (1992). "Estimation of land surface temperature with NOAA9 data." Remote Sensing of Environment **40**(1): 27-41.

Paw U, K. T. (1992). "Development of Models for Thermal Infrared Radiation Above and Within Plant Canopies." ISPRS Journal of Photogrammetry and Remote Sensing **42**: 19-203.

Peppler, R. A., P. J. Lamb, et al. (1996). "Site scientific mission plan for the southern Great Plains CART site: January–June 1996." National Technical Information Services Report: 86.

Peres, L. F. and C. C. DaCamara (2004). "Land surface temperature and emissivity estimation based on the two-temperature method: sensitivity analysis using simulated MSG/SEVIRI data." Remote Sensing of Environment **91**: 377-389.

Peres, L. F. and C. C. DaCamara (2006). "Improving two-temperature method retrievals based on a nonlinear optimization approach." IEEE Transactions on Geoscience and Remote Sensing **3**(2): 232-236.

Pinker, R., D. L. Sun, et al. (2009). "Evaluation of Satellite Estimates of Land Surface Temperature from GOES over the United States." Journal of Applied Meteorology and Climatology **45**: 167-180.

Prata, A. J. (1994). "Land surface temperatures derived from the advanced very high resolution radiometer and the along-track scanning radiometer. 2: Experimental results and validation of AVHRR algorithms." Journal of Geophysical Research **99**(D6): 13025-13058.

Prata, A. J. and R. P. Cechet (1999). "An assessment of the accuracy of land surface temperature determination from the GMS-5 VISSR." Remote Sensing of Environment **67**(1): 1-14.

Prata, A. J. and C. M. R. Platt (1991). Land surface temperature measurements from the AVHRR. Proc. 5th AVHRR Data Users Conference. Tromso, Norway**:** 438-443.

Price, J. C. (1984). "Land surface temperature measurements from the split window channels of the NOAA-7 AVHRR." Journal of Geophysical Research **79**: 5039-5044.

Running, S. W. (1991). Computer simulation of regional evapotranspiration by integrating landscape biophysical attributes with satellite data, in Land Surface Evaporation: Measurements and Parameterization. New York, Springer.

Running, S. W., C. Justice, et al. (1994). "Terrestrial remote sensing science and algorithms planned for EOS/MODIS." International Journal of Remote sensing **15**: 3587 - 3620.

Schadlich, S., F. M. Gottsche, et al. (2001). "Influence of land surface parameters and atmosphere on METEOSAT brightness temperatures and generation of land surface temperature maps by temporally and spatially interpolating atmospheric correction,." Remote Sensing of Environment **75**(1): 39-46.

Schmit, T. J., M. M. Gunshor, et al. (2005). "Introducing the next-generation Advanced Baseline Imager on GOES-R." Bulletin of the American Meteorological Society **86**: 1079-1096.

Schmugge, T., J. Becker, et al. (1991). "Spectral emissivity variations in airborne surface temperature measurements." Remote Sensing of Environment **35**: 95-104.

Sellers, P., F. Hall, et al. (1995). "The Boreal Ecosystem-Atmosphere Study (BOREAS): AN overview and early results from the 1994 field year." Bulletin of the American Meteorological Society **76**: 1549-1577.

Sellers, P. J., F. G. Hall, et al. (1992). "An overview of the First International Satellite Land Surface Climatological Project (ISLSCP) Field Experiment (FIFE)." Journal of Geophysical Research **97**(D17): 18345-18371.

Sellers, P. J., F. G. Hall, et al. (1997). "BOREAS in 1997: Experiment overview, scientific results, and future directions." Journal of Geophysical Research **102**(D24): 28731-28769.

Snyder, W. C., Z. Wan, et al. (1998). "Classification-based emissivity for land surface temperature measurement from space." international Journal of Remote Sensing **19**(14): 2753-2774.

Sobrino, J. A., Z. L. Li, et al. (1994). "Improvements in the split-window technique for land surface temperature determination." IEEE Transactions on Geoscience and Remote Sensing **32**(2): 243-253.

Sun, D. and R. Pinker (2003). "Estimation of land surface temperature from a Geostationary Operational Environmental Satellite (GOES-8)." Journal of Geophysical Research **10**(D11): 4326-.

Sun, D. and R. Pinker (2004a). "Case study of soil moisture effect on land surface temperature retrieval." iEEE Transactions on Geoscience and Remote Sensing Letters **1**(2): 127-130.

Sun, D. and R. T. Pinker (2007). "Retrieval of Surface temperature from the MSG_SEVIRI observations: Part I. Methodology." international Journal of Remote Sensing **28**(23): 5255-5272.

Sun, D., R. T. Pinker, et al. (2004b). "Land Surface Temperature Estimation from the Next Generation of Geostationary Operational Environmental Satellites: GOES M-Q." <u>Journal of Applied Meteorology and Climatology</u> **43**: 363-372.

Sun, D. L., R. Pinker, et al. (2006). "Diurnal temperature range over the United States: A satellite view." <u>Geophysical Research Letters</u> **33**: L05705.

Ulivieri, C. and G. Cannizzaro (1985). "Land surface temperature retrievals from satellite measurements." <u>Acta Astronautica</u> **12**(12): 985-997.

Ulivieri, C., M. M. Castronouvo, et al. (1992). "A SW algorithm for estimating land surface temperature from satellites." <u>Advances in Space Research</u> **14**(3): 59-65.

Vidal, A. (1991). "Atmospheric and emissivity correction of land surface temperature measured from satellite using ground measurements or satellite data." <u>international Journal of Remote Sensing</u> **12**(12): 2449-2460.

Wan, Z. (2008). "New refinements and validation of the MODIS Land-Surface Temperature/Emissivity products." <u>Remote Sensing of Environment</u> **112**: 59-74.

Wan, Z. and J. Dozier (1989). "Land-surface temperature measurement from space:physical principles and inverse modeling." <u>IEEE Transactions on Geoscience and Remote Sensing</u> **27**(3): 268 -- 278

Wan, Z. and J. Dozier (1996). "A generalized split-window algorithm for retrieving land-surface temperature from space." <u>IEEE Transactions on Geoscience and Remote Sensing</u> **34**(4): 892-905.

Wan, Z., Member of IEEE, et al. (1997). "A physics-based algorithm for retrieving land-surface emissivity and temperature from EOS/MODIS data." <u>IEEE Transactions on Geoscience and Remote Sensing</u> **35**(4): 980-996.

Watson, K. (1992a). "Spectral ratio method for measuring emissivity." <u>Remote Sensing of Environment</u> **42**: 113-116.

Watson, K. (1992b). "Two-temperature method for measuring emissivity." <u>Remote Sensing of Environment</u> **42**: 117-121.

Weinreb, M., M. Jamieson, et al. (1997). "Operational Calibration of the Imagers and Sounders on the GOES-8 and -9 Satellites." <u>Applied Optics</u> **36**: 6895-6904.

Witten, I. H. and E. Frank (2005). <u>Data Mining: practical machine learning tools and techniques. </u>. Boston,MA Morgan Kaufman.

Yu, Y., J. L. Privette, et al. (2008). "Evaluation of split-window land surface temperature algorithms for generating climate data records." <u>IEEE Transactions on Geoscience and Remote Sensing</u> **46**(1): 179-192.

Yu, Y., D. Tarpley, et al. (2009a). "Developing algorithm for operational GOES-R land surface temperature product." <u>IEEE Transactions on Geoscience and Remote Sensing</u> **47**(3): 936-951.

Yu, Y., H. Xu, et al. (2009). <u>A Simplified method for measuring land surface temperature and emissivIty using thermal infrared split-window channels</u>. IGARSS Annual meeting, Cape Town.

Zhang, L., R. Lemeur, et al. (1995). "A one-layer resistance model for estimating regional evapotranpiration using remote sensing data." <u>Agricultural and Forest Meteorology</u> **77**(3-4): 241-261.

Curriculum Vitae

Ms. Li FANG received her Bachelor of Science in Engineering in Geographic Information Systems from Wuhan University, Hubei, China, in 2005. She has four-year research experience in Chinese Academy of Sciences, Beijing, China from 2005 to 2009. In 2011, she received her Master of Science in Geographic and Cartographic Sciences from George Mason University.